# Metal fluxes across the sediment water interface in a drinking water reservoir

Kathryn Marie Krueger

Thesis submitted to the faculty of the Virginia Polytechnic Institute and State University in partial fulfillment of the requirements for the degree of

Master of Science

In

Geosciences

Madeline Schreiber, Committee Chair

Cayelan Carey

James Rimstidt

May 10, 2019

Blacksburg, VA

Keywords: iron, manganese, management, metals, reservoir

Metal fluxes across the sediment water interface in a drinking water reservoir

Kathryn Marie Krueger

## Abstract

Elevated concentrations of iron (Fe) and manganese (Mn) in drinking water degrade water quality by affecting taste, odor, and color. Under oxic conditions (dissolved oxygen (DO) >2 mg/L), Fe and Mn are rarely present in soluble form in natural waters, as they occur as insoluble, oxidized minerals in sediments. However, the development of low DO concentrations in the bottom waters of some lakes and drinking water reservoirs during thermal stratification can lead to the reduction of oxidized, insoluble Fe and Mn in sediments to soluble forms, which are then released into the water column. In response, many water utilities have installed oxygenation systems to control metal concentrations *in situ* in drinking water reservoirs. However, previous research has found anoxic (DO < 0.5 mg/L) conditions still develop within sediments, even with operational oxygenation systems, allowing for the reduction and release of soluble Fe and Mn into the water column.

To examine the drivers of metal release from sediments into the water column, I conducted sediment flux chamber experiments to directly quantify Fe and Mn fluxes at the sediment-water interface of a small, eutrophic drinking water reservoir (Falling Creek Reservoir, Vinton, VA). The experiments were conducted twice during the 2018 summer stratification period (April 24 – October 21). Using the flux chambers, I measured total and soluble Fe and Mn concentrations under changing oxygen conditions over 10-day periods to calculate fluxes. Throughout the experiments, I monitored DO, oxidation-reduction potential (ORP), temperature, and pH. In

addition to the direct measurements, I also estimated metal fluxes using a mass balance method, which relies on measurements of metal inputs and outputs into the bottom waters of the reservoir.

Overall, our results showed that fluxes are highly variable during the stratification period, with some periods having positive fluxes (release of metals from sediment to the water column) and some with negative fluxes (return of metals from the water column to sediment). The metal fluxes are highly sensitive to redox conditions in the water column, sediment-water interface and sediments.

Metal fluxes measured using the chambers are 91-105% higher than those estimated using the mass balance method. This difference supports result of previous work that the flux chamber method likely provides maximum values of metal fluxes as the isolated chamber water does not allow for mixing with the bottom waters. In contrast, because the mass balance method relies on water column data, results are affected by mixing and biogeochemical reactions that can remove metals from the water column; thus, flux estimates using this method likely reflect minimum values. However, when used together, these two methods provide a useful tool for constraining metal fluxes under different redox conditions and highlight the importance of measuring ORP in addition to DO. The results of this study can be used by water utilities to improve the effectiveness of engineered oxygenation systems and water quality management practices related to iron and manganese.

Metal fluxes across the sediment water interface in a drinking water reservoir

Kathryn Marie Krueger

## General Audience Abstract

In many drinking water reservoirs, elevated concentrations of metals, such as iron (Fe) and manganese (Mn), pose a challenging water quality problem. Elevated metal concentrations affect taste, color, and odor in drinking water and can be expensive to treat for. The presence of Fe and Mn in water is influenced by the oxygen concentrations in the water. When oxygen levels in the water are high, Fe and Mn are not soluble in water. However, when the oxygen levels in water are low, Fe and Mn can be released from soils, sediments and rocks into water and can thus pose a concern for drinking water quality. Many water utilities have installed systems to increase oxygen concentrations in drinking water reservoirs with the goal of maintaining low levels of metals in water supplies. However, previous research has shown that even when oxygenation systems are operational, Fe and Mn can still be released into water from the reservoir's bottom sediments.

To examine the factors that contribute to the release of metals from the sediments into the water column, I measured the rate of release of Fe and Mn from the sediments into the water column at a local drinking water reservoir (Falling Creek Reservoir, Vinton, VA). I conducted the experiments twice during summer 2018 using chambers that isolated the water immediately above the sediments. During the experiments, I monitored how Fe and Mn concentrations changed over time under different oxygen conditions. In addition to the measurements, I also used a mass balance method using water column data to estimate the metal release.

Overall, results showed that release rates are highly variable during the summer months, with some periods having positive rates (releasing metals from sediments into the water column) and some with negative rates (returning metals from the water column to sediment). The metal release rate are highly sensitive to oxygen conditions in the water column, at the sediment-water interface and in the sediments. When used together, these two methods provide a useful tool for constraining metal release rates under different oxygen conditions.

This research will help drinking water plant managers to improve the effectiveness of oxygenation systems and water quality management practices related to Fe and Mn. Additionally, this research will help improve the water quality for residents and can be applied to other lakes and reservoirs where metal concentrations are elevated.

## Acknowledgements

This work has been supported by: the Virginia Tech Institute for Critical Technology and Applied Science, the Virginia Tech Department of Geosciences, the Consortium of University for the Advancement of Hydrologic Science, Inc, the Virginia Tech Graduate Student Assembly, the Virginia Water Resource Research Center, the Geological Society of America, and the National Science Foundation.

Thank you to the Western Virginia Water Authority for allowing us access to the reservoir to conduct our studies. Thank you to Athena Tilley for analyzing the metal samples for this project. Thank you to the Carey Lab, specifically Cayelan, Ryan, Mary, and Bethany, for all of the support, mentorship, and friendship over the past couple of years. Thank you to the awesome undergraduate students that I got to work with, including Amanda Powers, Claire Vavrus, and Michael Zigah. Thank you to John Chermak for stepping in as a proxy committee member and giving valuable feedback on the project.

Thank you to Don Rimstidt, for answering countless questions on statistics and redox chemistry. I wish you could have seen the results of this project because it would not have gotten to this point if it wasn't for you.

Thank you to my parents: six years, two degrees, and four foot surgeries later, I would not be writing this thesis if it wasn't for the constant support you have provided. You have answered endless phone calls, moved in with me just to make sure I could continue school, and have listened to me ramble on about both the highs and the lows of this project. Thank you for making sure I could walk across the stage to accept my diploma, I really couldn't have done it without you two.

A finally, thank you Maddy for being the best advisor I could've ever hoped for. You took a chance on me when I was just a freshman walking into your office and I am forever grateful. I have learned so much from you, including how to be a better scientist and a better mentor. You have been such an amazing role model and it was an honor to have been able to work with you. Thank you for all of the ice cream and the long days on the boat together, I will never forget my time here.

## Table of Contents

## List of Figures and Tables

## Preface/Attribution

Authors:

Kathryn M. Krueger[1], Claire E. Vavrus[2], Mary Lofton[3], Ryan McClure[3], Paul Gantzer[4], Cayelan C. Carey[3] Madeline E. Schreiber[1]

[1]Virginia Tech Department of Geosciences

[2]University of Wisconsin – Madison Department of Geological Engineering and Geoscience

[3]Virginia Tech Department of Biological Sciences

[4]Gantzer Water Resources Engineering

- KMK, MES, and CCC developed original project idea.
- KMK and MES planned the flux chamber experiments
- KMK, CEV, and MES conducted the flux chamber experiments
- PG designed and provided technical help with flux chambers
- KMK, RPM, MEL, and CEV collected depth and inflow samples for the mass balance method
- KMK, RPM, and MES compiled and analyzed data
- KMK wrote the thesis in consultation with MES and CCC.

## 1.0 Introduction

Elevated concentrations of iron (Fe) and manganese (Mn) in drinking water degrade water quality by affecting taste, odor, and color (Du, 2004). In response, the U.S. Environmental Protection Agency (USEPA) established secondary drinking water standards for Fe and Mn in drinking water of 0.3 and 0.05 mg/L, respectively (USEPA, 2017). These metals are essential elements with minimum daily requirements ranging from 10 to 50 mg/d for Fe (World Health Organization, 1996) and 3.5 to 7 mg/d for Mn (World Health Organization, 2004). However, chronic exposure to elevated concentrations of Mn in drinking water has been associated with adverse health impacts, including neurological disorders in children (Bouchard et al., 2007; Bouchard et al., 2011; Khan et al., 2011; Oulhote et al., 2014; Wasserman et al., 2011). The U.S. EPA currently recommends a lifetime health advisory for Mn of 0.3 mg/L (Du, 2004).

Both Fe and Mn are naturally-occurring metals in the Earth's crust, with average soil contents of 38 g/kg of Fe and 0.545 g/kg of Mn (Pais and Jones, 1997). In soils, Fe exists mainly as oxides and hydroxides such as hematite ($Fe_2O_3$), magnetite ($Fe_3O_4$), and siderite ($FeCO_3$). Manganese is commonly found in oxide form such as pyrolusite ($MnO_2$), cryptomelane ($KMn_8O_{16}$) and manganite (MnO(OH)) (Pais and Jones, 1997). Iron and Mn have similar chemical properties and often co-occur in minerals (Groschen et al., 2009).

As both Fe and Mn are common constituents in soils and sediments, they are also often found in natural waters. Iron is commonly detected in fresh water at concentrations ranging from 0.04-6200 mg/L (Pais and Jones, 1997). Manganese is also commonly occurring in both surface water and groundwater with median concentrations 0.02 mg/L and 0.05 mg/L, respectively (World Health Organization, 2004). The U.S. Geological Survey National Ambient Water Quality Assessment program, which monitors approximately two-thirds of public water systems in the

U.S., found Mn in 97% of surface water sites and 62% of wells sampled in the study  A recent study by McMahon et al. (2019) reported approximately 2.6 million people (~7%) with private wells in the U.S. potentially consume groundwater with concentrations above the EPA's lifetime health advisory guideline (0.3 mg/L).

Both Fe and Mn occur in several oxidation states that influence their cycling in natural systems (Davison, 1993). Iron has two main oxidation states: Fe(II), the reduced form, is generally soluble in natural waters under neutral pH conditions and Fe(III), the oxidized form, can be complexed with other ligands (i.e. hydroxides, phosphates) and is generally stable in its mineral (insoluble) form (Langmuir, 1997). Manganese has two main oxidation states: Mn (II) is stable under suboxic to anoxic conditions and Mn (IV) oxides are thermodynamically stable under oxic conditions (Davison, 1993).

Because Fe and Mn have several oxidation states, they participate in coupled oxidation-reduction reactions.  Reduced forms of Fe and Mn can be electron donors and can be coupled with the oxidation of electron acceptors, such as oxygen or nitrate. Conversely, oxidized forms of Fe and Mn can be electron acceptors and coupled with the oxidation of electron donors such as organic matter.  These reactions can be predicted based on energy yielded by the reaction (often called the "redox ladder"). In abiotic conditions, Mn reduction is thermodynamically more favorable than Fe reduction, but Mn oxidation is less favorable than Fe oxidation (Langmuir, 1997). Reduction and oxidation of Fe and Mn species can also be mediated by many different species of microorganisms, who can couple these reactions to gain energy (Davison, 1993; Madigan et al., 1997).

In freshwater bodies, such as lakes and reservoirs, dissolved oxygen (DO) concentrations have a strong influence on Fe and Mn dynamics. Under oxic conditions (DO >2 mg/L), Fe and Mn occur in their oxidized, insoluble forms (e.g. Fe and Mn oxyhydroxides) in sediments (Davison,

1993). However, the development of low DO conditions in the hypolimnion of many lakes and reservoirs during summer thermal stratification leads to microbial reduction of Fe and Mn in the sediments, releasing reduced, soluble forms of Fe (Fe (II)) and Mn (Mn (II)) into the water column (Brannon et al., 1985; Davison, 1993; World Health Organization, 2004).

The high cost of treating water with elevated metal concentrations, coupled with the knowledge that metals are redox sensitive, has led many water utilities to use engineered hypolimnetic oxygenation (HOx) systems to control metal concentrations *in situ* in lakes and reservoirs used for drinking water (Bryant et al., 2011b; Gantzer et al., 2009; Gerling et al., 2014). The goals of operating HOx systems are to prevent metal release from the sediment by maintaining oxic hypolimnia and to oxidize and precipitate any soluble metals that are released into the water column.

However, even with HOx systems in place, anoxic (DO < 0.5 mg/L) conditions can still develop within sediments (Bryant et al., 2011a), which allows for reduced metals in sediment pore water to diffuse upward towards the sediment water interface (SWI). At the SWI, which represents a redox boundary between the anoxic sediments and the oxic water column, reduced Fe diffusing upward is oxidized, leading a layer of particulate iron (Fe (III)) at the boundary (Davison, 1993). Manganese behavior differs from that of Fe because it oxidizes more slowly and oxidation rates are controlled by pH (Davison, 1993). Thus, at the redox boundary, although Mn can oxidize to form solid-phase Mn, fluxes of reduced Mn into the overlying water column can still persist (Brannon et al., 1985).

Designing and implementing successful HOx systems require information on the oxygen demand of the water column and the underlying sediments (Gerling et al., 2014). Hypolimnetic oxygen demand is calculated as the rate of decrease of DO concentration in the water column of

the hypolimnion (Gerling et al., 2014). After thermal stratification sets up, hypolimnetic oxygen demand reflects a combination of both water column and sediment oxygen demand (SOD) (Adams et al., 1982). SOD, the consumption of DO in the sediments, contributes to the overall hypolimnetic oxygen demand (Walker and Snodgrass, 1986), making it an important parameter when designing HOx systems. For example, SOD has been estimated to be 18% and 40% of the total hypolimnetic oxygen demand in Hamilton Harbour of Lake Ontario (Polak and Haffner, 1978) and Lake Erie (Di Toro and Connolly, 1980), respectively.

Design of HOx systems also benefits from accurate measurement of metal fluxes from sediments to the water column (Adams et al., 1982), as reduced metals impart an additional oxygen demand. Metal flux measurements are used to quantify metal loads into the water column under different oxygen and temperature conditions, which is important for utilities so that they can treat the reservoir in a cost-effective manner. In addition, measurements of metal fluxes under varying oxygen conditions are useful for constraining metal processes and cycling in freshwater bodies. Last, they provide important inputs into water quality forecast models.

Metal fluxes across the SWI can be measured using both indirect and direct methods. Indirect methods include use of mass balance approaches and sediment core incubations. For the mass balance method, the inputs and outputs of metal loadings and the change in the hypolimnetic mass are used to estimate fluxes across the SWI (Belzile et al., 1996; Davison, 1993; Davison and Woof, 1984; Munger et al., 2016; Yagi, 1996). The main advantage of this method is that it can be used to estimate fluxes over long time periods at the ecosystem scale, assuming that measurements of the metal loadings are made over that period. However, this method cannot separate metal fluxes and the effects of complex physical and biogeochemical reactions occurring at the SWI which can lead to underestimating the metal fluxes (Belzile et al., 1996; Davison, 1981). To counter this

problem, several authors have suggested measuring a detailed profile of water chemistry within 25 cm of the sediments (Belzile et al., 1996; Carey and Rydin, 2011; Davison, 1981; Davison, 1993; Davison and Woof, 1984) to accurately characterize conditions at the SWI.

The second indirect method relies on laboratory incubations using sediment cores with hypolimnetic water collected immediately above the sediments (Beutel, 2003; Beutel et al., 2008; Brannon et al., 1985). These samples can be incubated under both oxic and anoxic conditions to measure how metal fluxes and SOD changes in response to water column oxygen concentrations. This method allows for easy manipulation of DO conditions during the incubations, allowing for both oxic and anoxic trials. However, it can overestimate fluxes due to the increased concentration gradient that develops when replacing the overlying water with dilute reagent water (Beutel et al., 2008). In addition, results from sediment cores incubated in the laboratory are difficult to scale up to the larger reservoir ecosystem (Bryant et al., 2010a).

Direct methods to measure fluxes include use of diffusion samplers and benthic flux chambers. *In situ* peepers, or diffusion samplers, can be used to measure a microprofile of metal concentrations across the SWI (Belzile et al., 1996; Bryant et al., 2011b; Bryant et al., 2012; Bryant et al., 2010b; Teasdale et al., 1995), which can be used to make direct measurements of metal fluxes from sediments into the water column (Bryant et al., 2011b). Peepers can maintain sample integrity and are relatively free from contamination; however, they require careful calibration and have a high risk of misuse (Teasdale et al., 1995). Additionally, they have limited vertical resolution which can lead to underestimating the concentration gradients near the SWI (Belzile et al., 1996). In addition, because peepers are deployed at only one site, if sediments are heterogenous, there is need for a large number of replicates in order to get a representative measure (Bryant et al., 2011b).

Benthic flux chambers also measure fluxes *in situ* across the SWI (Adams et al., 1982; Berelson and Hammond, 1986; Elrod et al., 2004; Pakhomova et al., 2007; Polak and Haffner, 1978; Tomaszek and Czerwieniec, 2000). Flux chambers provide a direct measurement of diffusive fluxes at the SWI by isolating the water immediately above the SWI from the surrounding water column. Other benefits include the ability to concurrently measure DO, pH, temperature, and oxidation-reduction potential (ORP) during experiments. Flux chambers have primarily been used in brackish and saltwater environments (Berelson and Hammond, 1986; Elrod et al., 2004; Pakhomova et al., 2007), but have also been deployed in freshwater systems (Adams et al., 1982; Polak and Haffner, 1978; Tomaszek and Czerwieniec, 2000). This method involves specialized equipment, requires extensive training and field work, and can generally only operate over short-term periods (days to weeks). Similar to other methods, flux chambers require replicates in order to get a representative measurement.

The goal of this study was to use multiple approaches to quantify metal fluxes across the SWI of a drinking water reservoir (Falling Creek Reservoir, located in Vinton VA) with an engineered oxygenation system under different biogeochemical conditions. I conducted field experiments at the reservoir using *in situ* benthic flux chambers to directly measure Fe and Mn fluxes at the SWI and compared results to an indirect method relying on mass balance calculations. My central hypothesis was that when the overlying water column is oxic (oxidizing), Fe and Mn fluxes from the sediments to the water column should be lower than when the overlying water column is anoxic (reducing; **Error! Reference source not found.**). I tested this hypothesis by m easuring metal fluxes under different biogeochemical conditions created by the combined effects of the HOx system and seasonal stratification.

## 2.0 Methods

### 2.1 Site Description

Falling Creek Reservoir (FCR; Figure 2) is a small (maximum depth = 9.3 m, mean depth = 4 m, surface area = 0.119 $km^2$, volume = 3.1x $10^5$ $m^3$ at full pond), eutrophic reservoir near Vinton, Virginia, USA (37° 18' 12"N, 79° 50' 14" W) (Gerling et al., 2014). The reservoir is owned and operated by the Western Virginia Water Authority. FCR historically exhibits thermal stratification from May to October, which leads to the development of anoxic conditions in the hypolimnion (Gerling et al., 2014; Munger et al., 2016). Inflow from the upstream tributary is the largest water input to FCR (Gerling et al., 2014), contributing 95% of inputs to the reservoir (Gerling et al., 2016).

In autumn 2012, a side-stream supersaturation hypolimnetic oxygenation system (HOx) was installed to increase DO concentrations in the hypolimnion of the reservoir while maintaining thermal stratification (Gerling et al., 2014). In 2018, when this study was conducted, the HOx system was fully operational (Table 1) from April 24 to July 19. From July 19 to July 30, the HOx system was only partially operational, indicated by low volume-weighted hypolimnetic (VWH) DO concentrations of less than 2 mg/L. The HOx system was then de-activated from July 30 to August 9. The system was re-activated on August 9; however, it was again only partially operational during this time with VWH DO concentrations less than 2 mg/L. The HOx system was de-activated again on September 11. The reservoir turned over (TO; de-stratified) on October 21.

### 2.2 Water Column Sampling

We collected water samples from FCR for total and soluble Fe and Mn concentrations weekly from May to October 2018 and monthly from November 2018 to April 2019. Water samples were collected along a depth profile (0.1, 1.6, 3.8, 5.0, 8.0, 9.0 m, the water treatment

extraction valve depths) at the deepest site in FCR (Figure 2). Unfiltered samples (total metals) were poured directly from a 4-L Van Dorn sampler (Wildlife Supply Company, Yulee, FL) into 15 mL centrifuge tubes. Samples for soluble metals were filtered using 0.45 µm nylon syringe filters. Total and soluble samples for metal analysis were preserved using 0.5 mL trace metal grade nitric acid to pH < 2. Samples were analyzed for Fe and Mn concentrations using an Inductively Coupled Plasma Optical Emission Spectrometer (ICP-OES, Thermo Electron X-Series) following APHA Standard Method 3125-B (APHA, 1998). Detection limits for this method are 0.004 mg/L for Fe and 0.001 mg/L for Mn.

Dissolved oxygen, temperature, and pH were measured at 0.1 m depth increments at the same site using a Seabird Electronics SBE 19plus high-resolution profiler (CTD). All CTD data are available in the Environmental Data Initiative (EDI) repository (Carey et al., 2019). Previous work by Gerling et al. (2014) showed that DO concentrations measured at the deepest site in the reservoir were representative of conditions throughout the reservoir.

### 2.3 Measuring Benthic Fluxes

Metal fluxes across the SWI were measured using two methods: hypolimnetic mass budget (indirect) and benthic flux chambers (direct). For the indirect method, we estimated the net release of Fe and Mn from the sediments into the hypolimnion using mass budget measurements of discharge and metal concentrations in the hypolimnion, following Gerling et al. (2016). Direct measurements of Fe and Mn fluxes and oxygen demand at the SWI were made using benthic flux chambers deployed at the deepest point of FCR.

#### 2.3.1 Hypolimnetic Metals Mass Budget

We calculated the hypolimnetic metals budget (Figure 3) at weekly intervals from May to October 2018 to estimate metal fluxes using:

$$\frac{dM}{dt} = Q_{in}[C_{in}] - Q_{out}[C_{therm}] \pm J \quad (1)$$

where $\frac{dM}{dt}$ is the change in the hypolimnetic mass (mg/d), $Q_{in}$ is the flow rate of the primary tributary (L/d), $Q_{out}$ is the flow rate across the thermocline, $C_{in}$ is the concentration of metals (mg/L) at inflow sampling site, $C_{therm}$ is concentration of metals (mg/L) at the thermocline depth and J is the estimated metal flux at the SWI. Positive values of J indicate that metals are released from the sediments into the water column; negative values of J indicate that metals are removed from the water column and returning to the sediments. We assumed that all water coming in from the tributary went directly to the hypolimnion (Gerling et al., 2016). Additionally, we assumed that $Q_{in}$= $Q_{out}$ as there was no change in water level in the reservoir and no flow over the dam. The water treatment plant did not extract any water from the reservoir during the monitoring period. We did not account for precipitation or evaporation as we were only examining the hypolimnion.

To determine the boundary of the hypolimnion, we calculated the thermocline depth (m) using temperature data taken using the CTD and the Lake Analyzer package in MATLAB (Read et al., 2011). Calculated thermocline depths had a median of 3.8 m (averaged 4.6 m ± 2) during the 2018 stratification period.

Inflow to the reservoir was measured using a rectangular weir with a notch width of 1.1 m installed at the primary inflow of FCR. An INW Aquistar PT2x pressure sensor (INW, Kirkland, WA) recorded water level at the weir every 15 minutes, which we used to calculate the flow rate into the reservoir, following Gerling et al (2014):

$$Q = K * (L - 0.2 * H) * H^{1.5} \quad (2)$$

where Q is the flow rate ($m^3$/min), K is 110.29, a unit conversion constant, L is the crest length of the weir (m), and H is the hydraulic head (water level) behind the weir (m) (Gerling et al., 2014). We averaged the flow to get an average weekly flow for each sampling week. Total and

soluble samples for metal analysis, in addition to temperature and DO measurements, were collected weekly at the inflow stream, to yield a weekly average $C_{in.}$

The flow rate out of the hypolimnion across the thermocline was assumed to be equal to the flow rate into the reservoir for the 2018 stratification period, because there was no change in water levels of the reservoir and no water was removed for drinking water treatment. (Figure 3). To calculate the entrained metal load across the thermocline, we used the metal concentration at the average depth (3.8 m) of the thermocline for 2018.

To calculate $\frac{dM}{dt}$, we first calculated the total mass of metals in the hypolimnion using metals concentrations in samples collected from the four depths of the hypolimnion (5.0, 8.0, 6.2, and 9.0 m) multiplied by the layer volume of the depth from which they were sampled (Figure 3) and then summed to find the total hypolimnetic metal mass. In a similar fashion, SOD was calculated using the change of oxygen mass in the hypolimnion ($\frac{dM}{dt}$). The SOD estimated using the indirect mass balance method was sensitive only to HOx system operation as hydrologic inputs were not considered (Gerling et al., 2014).

The volume of the hypolimnion was calculated using bathymetry data that was interpolated using kriging interpolation techniques in ArcGIS (10.5.1). The area of the SWI was taken as the 3-D surface area of the reservoir below the average thermocline (3.8 m). The layer volume was calculated as the difference between the reservoir volume at the sample depth and the reservoir volume at the sampling depth immediately below (Figure 3).

To determine the change in metals mass each week, we subtracted the hypolimnetic mass of the preceding week, and then divided by 7 days (period between sampling dates). To get the flux per unit area of the reservoir, we divided the total hypolimnetic flux (mg/d) per week by the area of the SWI ($m^2$) of the hypolimnion.

### 2.3.2 Benthic Flux Chambers

To measure metal fluxes at the sediment-water interface, three benthic flux chambers (Figure 4, 5), similar to those described by Hicks (1990), were deployed at deepest site in FCR (Figure 2) during the 2018 season. The flux chambers isolated 24 cm of hypolimnetic water above the sediments and 0.27 $m^2$ of the SWI, for a total volume of 64.86 L of hypolimnetic water enclosed within the chambers.

We conducted two, ten-day experiments in 2018 (June 21 – July 2 and August 13 – 23) to examine the effects of different initial DO conditions on metal fluxes. During the June experiment, the HOx system was fully operating, creating high DO (7 mg/L, ~71% saturation) initial conditions in the hypolimnion. Before the August experiment, the HOx system was de-activated (Table 1), leading to lower initial DO (2 mg/L, ~18% saturation) conditions. Another difference between the two experimental periods was temperature; average temperature was 1°C higher in the hypolimnion in August than it was in June.

During the two experiments, we collected samples for total and soluble Fe and Mn every 3-4 days and also periodically checked Fe and Mn concentrations in the field using a Hach test kit. To sample the chamber, we first flushed the chamber tubing for one minute with chamber water; we then collected 15 mL of unfiltered water for total metals analysis and an additional 15 mL of filtered (0.45µm) water for soluble metals analysis. During both experiments, a maximum of 100 mL of chamber water was withdrawn at each sampling event to minimize the effects of removing chamber water on the chemical diffusion gradient within the chamber.

The chambers were attached to a pump to circulate the water within the chamber so that measured concentrations were representative of the entire chamber volume (Tengberg et al., 2005). During our experiments, chamber water was circulated for 2.5 minutes every 20 minutes. DO,

temperature, pH, and oxidation-reduction potential (ORP) probes were installed within the chambers to allow for high-frequency (2 minute) monitoring of biogeochemical conditions within the chambers during experiments.

During deployment, the three flux chambers were carefully lowered from a boat into the water column to not disturb the sediments and were seated at the deepest point of the reservoir (Figure 2). After deployment, the chambers were allowed to equilibrate for at least 24 hours. A few hours before each experiment, the flux chambers were flushed with hypolimnetic water for approximately 90 – 120 minutes until chamber DO concentrations and temperature stabilized and reflected the surrounding hypolimnetic conditions. We used the DO data to check if the flux chambers were properly deployed. If the chamber was not properly sealed, the DO within the chamber would increase during pumping or sampling, indicating that surrounding hypolimnetic water was being pulled into the chamber. If that occurred, we pulled the chamber and re-seated it in a nearby location.

In addition to the flux chambers, we also deployed one "water column" chamber in the hypolimnion, which had the same construction specifications as the flux chambers but was isolated from the sediments to account for changes in metal concentrations in the water column that were not associated with fluxes across the SWI. This chamber was deployed for the same interval as the flux chambers in the August experiment.

Metal fluxes for each chamber in each experiment were calculated using the following equation:

$$J = b * \left(\frac{V}{A}\right) \quad (3)$$

where J is the flux of the soluble or total metal $\left(\frac{\frac{mg}{m^2}}{day}\right)$, b is the slope of the line of best fit of the soluble or metal concentrations (mg/L/day), V is the volume of the flux chamber (64.86 L), and A is the surface area of the flux chamber (0.27 $m^2$).

SOD was measured as the rate at which DO depletes between the start of the experiment (hypolimnetic conditions) until DO <0.5 mg/L. SOD for each chamber in each experiment was calculated using the following equation:

$$J_{SOD} = b * \left(\frac{V}{A}\right) \quad (4)$$

where $J_{SOD}$ is the SOD $\left(\frac{\frac{mg}{m^2}}{day}\right)$, b is the slope of the line of best fit of the DO concentrations (mg/L/day), V is the volume of the flux chamber (64.86 L) and A is the surface area of the flux chamber (0.27 $m^2$).

Fluxes measured during the June and August experiments were compared with the fluxes estimated by the mass balance method with a non-parametric Wilcoxon rank sum test using JMP Pro 14. Significance was set at p-value < 0.05.

## 3.0 Results

### 3.1 DO, ORP, Temperature, pH conditions in FCR

FCR began to thermally stratify in April and remained stratified through fall turnover in late October 2018 (Figure 6). Prior to stratification, DO concentrations and temperatures were relatively uniform with depth through the water column of FCR. By the beginning of May, a thermocline developed at 3.8 m (Figure 6). Throughout the stratified period, the median thermocline depth was calculated to be at 3.8 m (Figure 6).

Within the hypolimnion, the DO concentrations were controlled by the operation of the HOx system. When the HOx system was fully operational between April and July (Table 1), volume-weighted hypolimnetic (VWH) DO concentrations were maintained at 4.7±0.36 mg/L (1 standard deviation) and DO near the SWI was > 2 mg/L (Figure 10). However, when the HOx system was partially operational (July 19 – July 30), VWH DO concentrations decreased to 1.75 mg/L. Once the HOx system de-activated on July 30, VWH DO concentrations decreased to 0.46 mg/L and DO conditions near the SWI became anoxic. The HOx system was turned back on August 19 but was only partially operational; during this time, VWH DO was 0.26±0.47 mg/L with fully anoxic conditions at the SWI. When the HOx system was de-activated for the last time in September, VWH DO remained low at 0.25 mg±0.39 mg/L until turnover (Figure 10).

On average, the water column was more oxidizing (30% higher ORP, at 199.7±11.0 mV) when the HOx system was fully operational compared to the rest of the stratification period (Figure 10). ORP at the SWI was lowest (1.4 mV) when the HOx system was de-activated. When the HOx system was partially operational in August-September, ORP at the SWI increased immediately following turning on the HOx system. However, within a week, ORP (and DO concentrations) decreased to levels preceding partial HOx operation. Immediately before the HOx system was de-

activated for the last time in September, conditions at the SWI became oxidizing (266 mV) despite DO concentrations < 2 mg/L (Figure 10).

The pH in the hypolimnion remained at 6 to 7 throughout the stratification period (Figure 10). Temperature in both the hypolimnion and at the SWI increased during the stratification period (Figure 10), with VWH temperature peaking in late September at 17.4 °C. At the time of the June experiment, the SWI temperature was 10.6°C, and at the time of the August experiment, the SWI temperature was 12.0°C. The peak SWI temperature of the stratification period was 13°C on September 24.

### 3.2 Hypolimnetic Mass Balance

#### 3.2.1 Fe and Mn loading

In the early stratification period (May – June) inflow (5.1±2.8 ML/d) was 94% higher than the low inflow period (0.32±0.44 ML/d) of July-September. In October, immediately before turnover, inflow (4.7±0.4 ML/d) was also high (93% higher than the preceding low inflow period; Figure 8) to the reservoir. During the May-June high inflow period, the hypolimnion experienced high input loading of total metals with low export of metals. During the October high inflow period, the hypolimnion received high input of metals but also exported metals (Figure 9).

#### 3.2.2 Hypolimnetic Fe and Mn mass

Total Fe and Mn mass increased in the hypolimnion during the summer stratified period regardless of oxygenation (Figure 7, 9). Excluding one week in May, total Mn (TMn) fractions were dominated by soluble Mn (SMn) throughout the stratified period, with 73%-100% of total Mn concentrations comprised of soluble Mn. Total Fe (TFe) concentrations were dominated by particulate forms until September (HOx system off), after which total Fe concentrations were comprised of 41-96% soluble Fe.

When the HOx system was fully operational, metal concentrations in the water column were lower than observed during the rest of the thermally stratified period (Figure 7, 10) and were sensitive to hydrologic inputs (Figure 9), with negative soluble metal fluxes when hydrologic inputs were high (Figure 11). During HOx operation, total and soluble Fe increased 6.8±1.5 kg/d and 1.3±0.5 kg/d respectively. During this time, VWH total and soluble Mn concentrations increased 4.1±0.55 kg/d and 3.6±0.54 kg/d, respectively.

When the HOx system de-activated in July, VWH total and soluble Fe increased to 2.1 and 0.3 mg/L respectively within two weeks. Regardless of HOx system operation, total and soluble VWH Fe concentrations continued to increase at rates of 10.3 ±1.8 kg/d and 8.0±2.0 kg/d throughout the stratification period to maximum concentrations of 4.6 and 4.3 mg/L, respectively, in October. During this time, total and soluble VWH Mn concentrations increased to 0.77 and 0.76 mg/L, respectively, within two weeks. Total and soluble VWH Mn concentrations remained between 0.54 to 0.77 mg/L for the rest of the stratification period until fall turnover, at which time there was a sharp decrease associated with reservoir mixing (Figure 10).

Total and soluble metal concentrations at the SWI were more sensitive to HOx operation and ORP changes than VWH metal concentrations. Total and soluble SWI Fe concentrations decreased 64 and 67%, respectively, while total and soluble SWI Mn both decreased by 42% when there was a 65% increase in SWI ORP in September. Following the decline of ORP to previous levels, total and soluble SWI Fe and Mn concentrations began to increase (Figure 10). Additionally, SWI total Fe concentrations increased to 42-94% higher concentrations than the VWH concentrations. Soluble Fe at the SWI was 4% lower than VWH soluble Fe in September, but otherwise, SWI soluble Fe was 22-97% higher than VWH concentrations (Figure 10). Total

and soluble SWI Mn concentrations were 42-93% and 41-94% higher, respectively, than VWH concentrations (Figure 10).

### 3.2.3 Fe and Mn fluxes between sediments and hypolimnion

Fluxes across the SWI estimated using the mass balance method were highly variable throughout the stratification period and included both positive (net release) and negative (net return) metal fluxes. Total and soluble Fe fluxes included both positive and negative values (-559 to 408 mg/m$^2$/d for total; -695 to 392 mg/m$^2$/d for soluble). Similarly, total and soluble Mn included positive and negative values, ranging from -96 to 61 mg/m$^2$/d (total) and -99 to 62 mg/m$^2$/d (soluble). On average, we observed a net release (positive J; eq 2) of total and soluble Fe (3.8±175 and 14.0±200 mg/m$^2$/d, respectively) and a net release of total and soluble Mn (0.70±30 and 3.8±30 mg/m$^2$/d, respectively) from the sediments into the hypolimnion (Figure 11).

When the HOx system was fully operational in May-July, average total Fe fluxes were negative (mean: -18.8±74 mg/m$^2$/d) from May - June, but in July total Fe fluxes became to positive (release from sediments; Figure 11). Soluble Fe fluxes were positive (mean: 2.3±17 mg/m$^2$/d) when the HOx system was fully operational but switched to negative values when the HOx system began to malfunction in July. After this malfunctioning period, average soluble Fe fluxes were positive for the rest of the stratification period. Total and soluble Mn fluxes were more variable when the HOx system was fully operational, with an overall net release of total and soluble Mn (5.5±22 and 10.1±18 mg/m$^2$/d, respectively) from the sediments into the hypolimnion during the oxygenated period.

During this time when the HOx was fully operational, metal fluxes also showed sensitivity to hydrologic inputs. When inflow from the primary tributary to the hypolimnion exceeded 2

ML/d, fluxes of total and soluble Fe, as well as total Mn, were negative (Figure 8,11). In contrast, soluble Mn fluxes were positive regardless of flow (Figure 8,11).

When the HOx system was de-activated on July 30, metals were released to the water column from sediments (Figure 11). During and after this time, soluble Fe fluxes into the water column remained positive until September. Similarly, total Fe fluxes were positive except for a week in August during which they shifted to negative (-45.7 mg/m$^2$/d). Total and soluble Mn fluxes also shifted to negative values during the partial operation of the HOx system from August 9 to September 11 (mean: -8.6±15.9 mg/m$^2$/d and -7.5±16.5 mg/m$^2$/d, respectively), signifying a return to the sediments.

When the HOx system was de-activated for the last time in September, total Fe and Mn fluxes (-64.0 mg/m$^2$/d and -4.2 mg/m$^2$/d) were initially negative, but became positive after one week. After the HOx system as off, soluble Fe and Mn fluxes (mean:214.5±136.7 mg/m$^2$/d and 12.1±14.8 mg/m$^2$/d respectively) remained positive until immediately before turnover. After turnover (21 October; Table 1), metal fluxes were once again negative.

The calculated Fe and Mn fluxes show a sensitivity to changes in SWI ORP in the water column (Figure 11). For example, the 173 mV increase in SWI ORP observed from August 27 to September 17 (Figure 10) was associated with negative fluxes of soluble and total Fe and Mn (Figure 11). And when ORP increased again in October due to a weakening thermocline immediately before turnover, total and soluble Fe and Mn fluxes were again negative, leading to the return of Fe and Mn to the sediments immediately before and after turnover.

**3.3 Benthic Flux Chambers**

Iron fluxes measured during the chamber experiments ranged from 290 to 672 mg/m$^2$/d and 255 to 594 mg/m$^2$/d for total and soluble forms, respectively (Figure 12). As suggested by the

wide range in measured flux values, there was considerable variability between the replicates of the flux chamber experiments, reflected by the coefficient of variation (CV) of 85% for both total and soluble Fe fluxes. There was no statistical difference in Fe fluxes between the June and August experiments (Wilcoxon rank sum test: $\chi_1^2$ = 3.0, p = 0.08; Table 2). Total Fe concentrations in the experimental samples were composed of 57±33% soluble Fe.

Manganese fluxes measured during the chamber experiments ranged from 28 to 88 mg/m$^2$/d and 29 to 89 mg/m$^2$/d for total and soluble Mn, respectively (Figure 12). Similar to Fe, there was variability between replicates of the flux chamber experiments for the Mn measurements, as reflected by the coefficient of variation (CV) of 102% for both total and soluble Mn. Also similar to Fe, there was no statistical difference in Mn fluxes between the June and August experiments (Wilcoxon rank sum test: $\chi_1^2$ = 0.33, p = 0.5; Table 2). Almost all the Mn (98±0.04%) was in soluble form.

Sediment-water interface DO concentrations measured using flux chambers were used to calculate SOD (Eq 3). The average SOD was 501 ± 383 mg/L (maximum of 1203 mg/L) during the study period (Figure 13). Although the initial DO concentrations between the June and August experiments were different (VWH DO in June and August was 8 and 2 mg/L, respectively), a comparison of the two experiments showed the rate of oxygen depletion was not statistically different (Wilcoxon rank sum test: $\chi_1^2$ = 0, p = 1.0; Table 2).

Fluxes of total and soluble Fe and Mn in the chamber experiments increased as SOD increased (Figure 13). Excluding one outlier for a flux chamber during the August experiment, the highest total and soluble Fe fluxes (672±51 and 594±128 mg/m$^2$/d, respectively) were measured when SOD was also the highest (1203±7 mg/m$^2$/d). Similarly, excluding one outlier (during June

experiments) soluble and total Mn fluxes were highest (ranging between 35 and 37 mg/m$^2$/d for both total and soluble Mn) when SOD was elevated (greater than ~ 450 mg/m$^2$/d; Figure 13).

ORP values measured during the experiments reflect reducing conditions; they reached a minimum of -300 mV to -410 mV for the June and August experiments, respectively. During the experiments, the ORP decreased, exhibiting small plateaus (Figure 12) over periods of between 0.5 to 6 days that were often associated with sharp increases in metal concentrations. Temperature and pH remained between 12 to 15°C and 6.3-7.6 respectively throughout both experiments (Figure S7).

For all experiments, the water column chamber measured negligible changes in soluble and total Fe and Mn concentrations (Figure S6), suggesting that the biogeochemical reactions affecting metal cycling in the hypolimnion were focused at the SWI. In addition, all or nearly all oxygen demand measured in the flux chambers can be attributed to SOD as the water column chamber measured a negligible oxygen demand (Figure S6).

### 3.4 Comparison of Direct and Indirect Methods for Estimating Fluxes

Metal fluxes measured using the flux chambers were consistently higher than fluxes estimated using the mass balance (Figure 14). For Fe, chamber-measured fluxes for total and soluble Fe were 504±149 mg/m$^2$/d and 472±138 mg/m$^2$/d, respectively; during the same time periods as the chamber experiments (June 21 to July 2 and August 13 to August 23), the Fe fluxes estimated using mass balance were 19±44 mg/m$^2$/d and 43±96 mg/m$^2$/d (total and soluble, respectively) (Figure 14). Comparison of the chamber-measured iron fluxes to the mass balance estimated fluxes showed that they are statistically different (Wilcoxon rank sum test: $\chi_1^2$ = 6.8, p = 0.009; Table 2).

Similarly to Fe, chamber-measured fluxes for total and soluble Mn were 44.9±25 mg/m$^2$/d and 45±25 mg/m$^2$/d, respectively, while the mass balance method estimates for total and soluble Mn fluxes were -1.9±21.4 mg/m$^2$/d and -2.3±20.8 mg/m$^2$/d, respectively. Similar to iron, comparison of the chamber-measured manganese fluxes to the mass balance estimated fluxes showed that they are statistically different (Wilcoxon rank sum test: $\chi_1^2$ = 6.8, p = 0.009; Table 2).

## 4.0 Discussion

In the following sections, we discuss the effects of redox conditions on Fe and Mn fluxes across the sediment-water interface. Additionally, we compare the methods used in this study and present study limitations.

### 4.1 Metals fluxes are sensitive to redox conditions

Overall, the flux measurement results support the initial hypothesis about the relationship between metal fluxes with redox conditions in the water column, SWI and the sediments (Figure 1). When the water column at the SWI (9 m) was more reducing (i.e. lower ORP and DO), Fe and Mn fluxes estimated from mass balance were higher than when the overlying water column was more oxidizing (Figure 11). Our flux chamber results also supported this, showing that Fe and Mn fluxes increased as DO concentrations and ORP declined (Figure 12).

The changes in ORP (Figure 12) during the flux chamber experiments reflect how quickly the redox conditions changed the chamber over the scale of days. At the start of the June experiment (Figure 12), the ORP data combined with the metal concentration data suggest that the water/sediment isolated by the flux chamber was under Mn reducing conditions (Langmuir, 1997), as there was an increase in Mn concentrations but no difference in Fe concentrations between the first two sampling points. After DO within the chamber depleted, concomitant with a decrease in ORP, our data suggest that the water/sediment reached Fe reducing conditions, leading to a positive flux of Fe (Figure 12).

In the August experiment, initial conditions within the flux chamber were more reducing. Since the HOx system was de-activated four days before the experiment started, both the water column and sediment were anoxic at the start of the experiment (Figure 10). At this time, ORP and metals data suggest that sediment was likely under Fe reducing conditions when the experiment

began (Figure 12). However, even under anoxic conditions, the higher concentrations of total Fe than soluble Fe (Figure 12) reflect that Fe is being oxidized, even in the absence of DO, suggesting the presence of another oxidant, likely Mn (IV) (Davison, 1993).

Estimated metal fluxes from the mass balance method were also sensitive to changes in overlying water column redox conditions (Figure 11) even though the reservoir water column did not reach as strongly reducing conditions as the flux chambers (Figure 14). While flux chamber waters reached negative ORP levels, VWH and SWI ORP measured in the water column (outside of the chambers) never dropped below 0 mV, suggesting that as soon as sediment pore water diffuses into the water column, it is mixed with more oxidizing water (Figure 10).

Iron and Mn fluxes estimated using the mass balance method were variable, with consistently positive fluxes during periods of reducing conditions (both low ORP and low DO). The largest Mn fluxes, in addition to strong positive Fe fluxes, occur as the SWI DO and ORP begin to decrease rapidly in July (Figure 11). After two weeks, the fluxes decrease despite continued low SWI DO and ORP. This can be attributed to a weakened concentration gradient at the SWI as Mn concentrations increase in the water column, leading to smaller diffusive fluxes (Bryant et al., 2011b). After July, hypolimnetic water conditions continue to become more reducing and SWI DO concentrations remain < 2 mg/L for the rest of the stratification period (Figure 10). During this time, despite low SWI DO, metal fluxes were still variable, with negative fluxes during more oxidizing conditions (high ORP) and positive fluxes during more reducing conditions (low ORP; Figure 11).

Despite anoxic conditions at the SWI from August until turnover, ORP increased twice during the stratification period, once in early August and again in late August (Figure 10). ORP initially increased on August 9 with the re-activation the HOx system, but quickly dropped as the

HOx system was unsuccessful at creating oxidizing conditions in the hypolimnion of FCR (Figure 6, 10). ORP sharply increased again in late August, despite no known change in HOx operation or in SWI DO concentrations (Figure 10). Both increases in ORP are associated with a decrease in water column Fe and Mn concentrations (Figure 10) and a negative flux (or return to the sediments) of metals (Figure 11).

When the HOx system was deactivated again on September 11, Fe and Mn fluxes become positive and increased until right before turnover. At turnover (October 21), the fluxes became negative, likely in response to mixing of oxic epilimnetic and anoxic hypolimnetic waters.

**4.2 Indirect estimates of fluxes are consistently lower than those measured directly**

A central goal of this study was to compare metal fluxes measured by the flux chamber method to those estimated by the hypolimnetic mass balance method. Metal fluxes and SOD measured with the flux chamber were consistently higher than those calculated using the mass balance method (Figure 14). This comparison supports work by previous authors that the flux chamber method measures the maximum metal fluxes across the SWI as the isolated chamber water does not allow for mixing with the rest of the hypolimnion (Adams et al., 1982). In contrast, because the mass balance method relies on water column data, results are affected by mixing and biogeochemical reactions that can remove metals from the water column; thus flux estimates using this method will reflect minimum values (Belzile et al., 1996).

Each method has its own sources of variability and uncertainty. The main source of variability in flux chamber measurements is related to the differences in replicate measurements, which is influenced by placement of the chambers and how well the chamber was sealed, as well as slight differences in sediment and pore water characteristics. Results of metal and DO concentrations, as well as ORP values, showed variability even between the replicates (Figure 13).

For the mass balance method, results had inherently higher uncertainty due to error propagation as each variable measured had its own associated error. However, even with these uncertainties, when used together, these two methods provide a useful tool for constraining the metal fluxes, which is important for both quantifying metal cycles and forecasting when net metal releases will occur.

**4.3 Metal fluxes in FCR are comparable to other lakes/reservoirs**

There have been other studies on metal fluxes in lakes/reservoirs, but these studies have used different methods under different biogeochemical conditions and over different time periods (Table 4), so a direct comparison of our results to these studies is challenging.

Overall, the chamber-measured Fe fluxes in FCR are higher than those measured in other studies, while estimates using the mass balance are comparable (Table 4). For example, our soluble Fe fluxes measured with the flux chambers (472±124 mg/m$^2$/d) are 60% higher than the range of soluble Fe flux estimates of 10-190 mg/m$^2$/d made by Belzile et al. (1996), Davison (1993), and Urban et al. (1997) while estimates from the mass balance (46±126 mg/m$^2$/d) fall within the range of the other studies. Similarly, our flux chamber total Fe fluxes (504±133 mg/m$^2$/d) are 81% higher than the total Fe fluxes of 0-66 mg/m$^2$/d estimated by (Brannon et al., 1985; Davison and Woof, 1984) while our mass balance estimated a total Fe flux of 29±125 mg/m$^2$/d, which is also within the range of the other studies. Our flux results may be on the higher end of the ranges found by other studies because the underlying geologic units in the region of FCR are crystalline rocks that contain Fe bearing minerals (Woodward, 1932).

Unlike Fe, Mn fluxes measured in FCR, regardless of the method, were comparable to fluxes measured in other studies (Table 4). Our soluble Mn fluxes measured with chambers (45±22 mg/m$^2$/d) and mass balance (8±21 mg/m$^2$/d) fall within the range of soluble Mn fluxes (1-126 mg/m$^2$/d) found in other studies (Belzile et al., 1996; Davison and Woof, 1984; Yagi, 1996).

Similarly, our total Mn fluxes from flux chambers (45±22 mg/m$^2$/d) and mass balance (5±21 mg/m$^2$/d) were in the same range of 10-39 mg/m$^2$/d estimated by Brannon et al. (1985) and Bryant et al. (2011b).

**4.4 Study Limitations**

Both the direct flux chamber method and the indirect mass balance method have limitations. The Fe and Mn fluxes estimated using the mass balance were calculated using many variables (i.e. thermocline depth, hydrologic inputs, pre-existing water column concentrations), each with their own errors, leading to error propagation. In addition, the effects of the HOx system are difficult to disentangle from the high inflow events in the mass balance, making it hard to differentiate between hydrologic and redox drivers of fluxes. Furthermore, the mass balance calculations are based on the thermocline depth (which affects the hypolimnetic volume, SWI surface area etc.). For the purpose of this study we used an average thermocline depth of 3.8 m for the 2018 stratification period; however, the thermocline changes over the course of the stratification period as the water column continues to warm (Figure 6).

With respect to the flux chamber experiments, the results can be difficult to scale up to the reservoir as it assumes that the fluxes across the entire SWI are homogenous, which is likely not the case (Steefel et al., 2005). The flux chambers are also logistically challenging to deploy, require specialized equipment, and thus only allow for a limited number of experiments, leading to low statistical strength when evaluating the results.

## 5.0 Conclusions

The primary goal of this study was to quantify metal fluxes across the SWI of a drinking water reservoir with an engineered oxygenation system under different biogeochemical conditions. Overall, our results showed that fluxes are highly variable during the stratification period, with some periods having positive fluxes (release of metals from sediment to the water column) and some with negative fluxes (return of metals from the water column to sediment). The fluxes are highly sensitive to redox and DO conditions in the overlying water column. We observed changes in fluxes associated with fluctuations in ORP when DO was fully depleted. These observations suggest that when the reservoir is anoxic, ORP is a useful parameter as an indicator of potential increases in metal fluxes into the water column.

Our results also show that using multiple methods for estimating fluxes is useful for quantifying the dynamics of metal exchange between sediments and the water column in reservoirs with engineering oxygenation systems. Through the comparison of the two methods we used to measure/estimate fluxes, we found that flux chambers measured higher metal fluxes than the mass balance method, but both methods in parallel provided complementary information for oxygenation system operation.

**Figures**

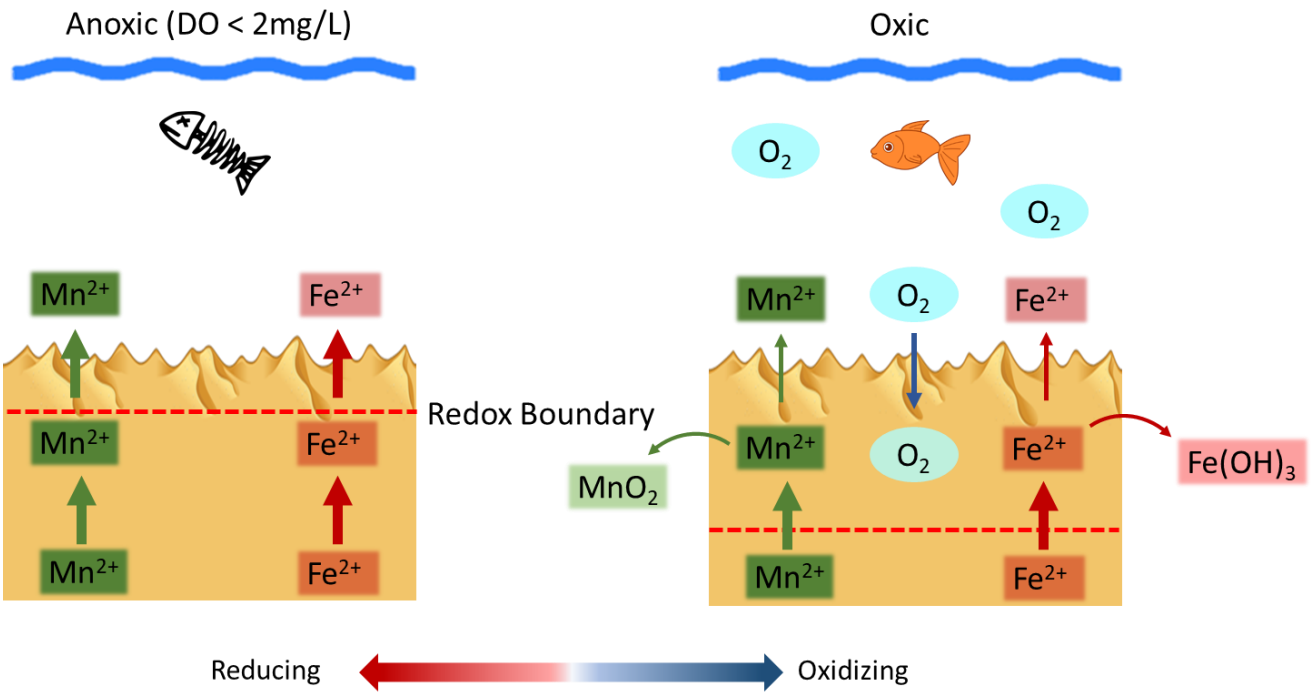


**Figure 1.** Central hypothesis in this study: when the overlying water column is oxic (right), Fe and Mn fluxes from the sediment pore water to the water column should be lower than when the overlying water column is anoxic (left).

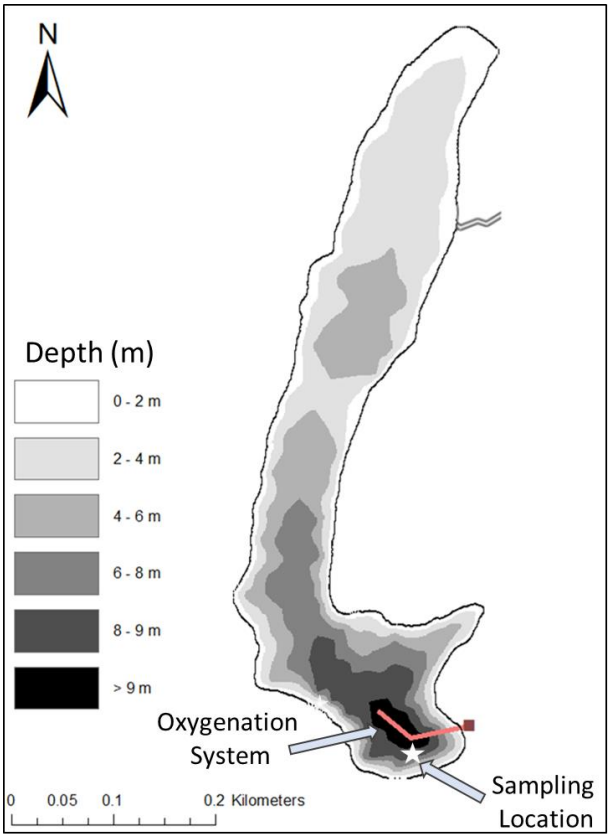


**Figure 2.** Bathymetry map of Falling Creek Reservoir, located in Vinton, VA, USA. The flux chambers and water column samples were taken at the deepest point of the reservoir. Also shown is the location of the oxygenation system and the primary inflow to the reservoir.

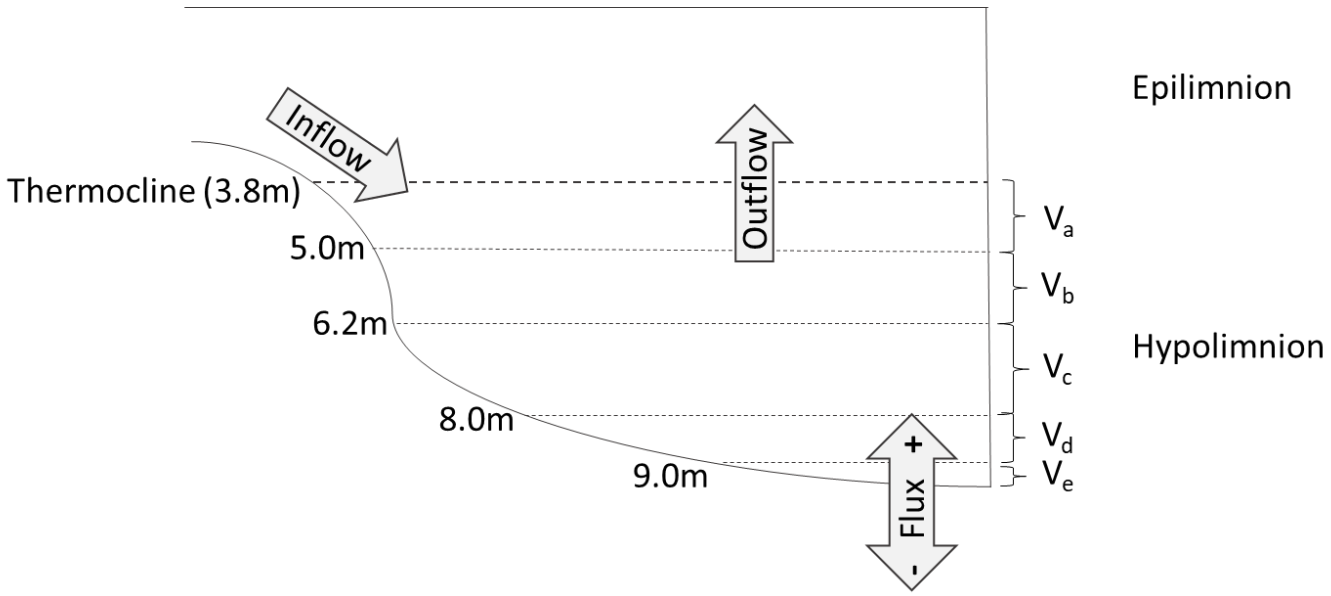


**Figure 3.** Conceptual model showing set-up of the hypolimnetic metals mass balance, including inputs, outputs and the exchange/flux between the water column and sediments. Volume layers ($V_{a-e}$) were calculated as the difference between volume of the reservoir at sample depth and the volume of the reservoir at the sampling depth immediately below**.**

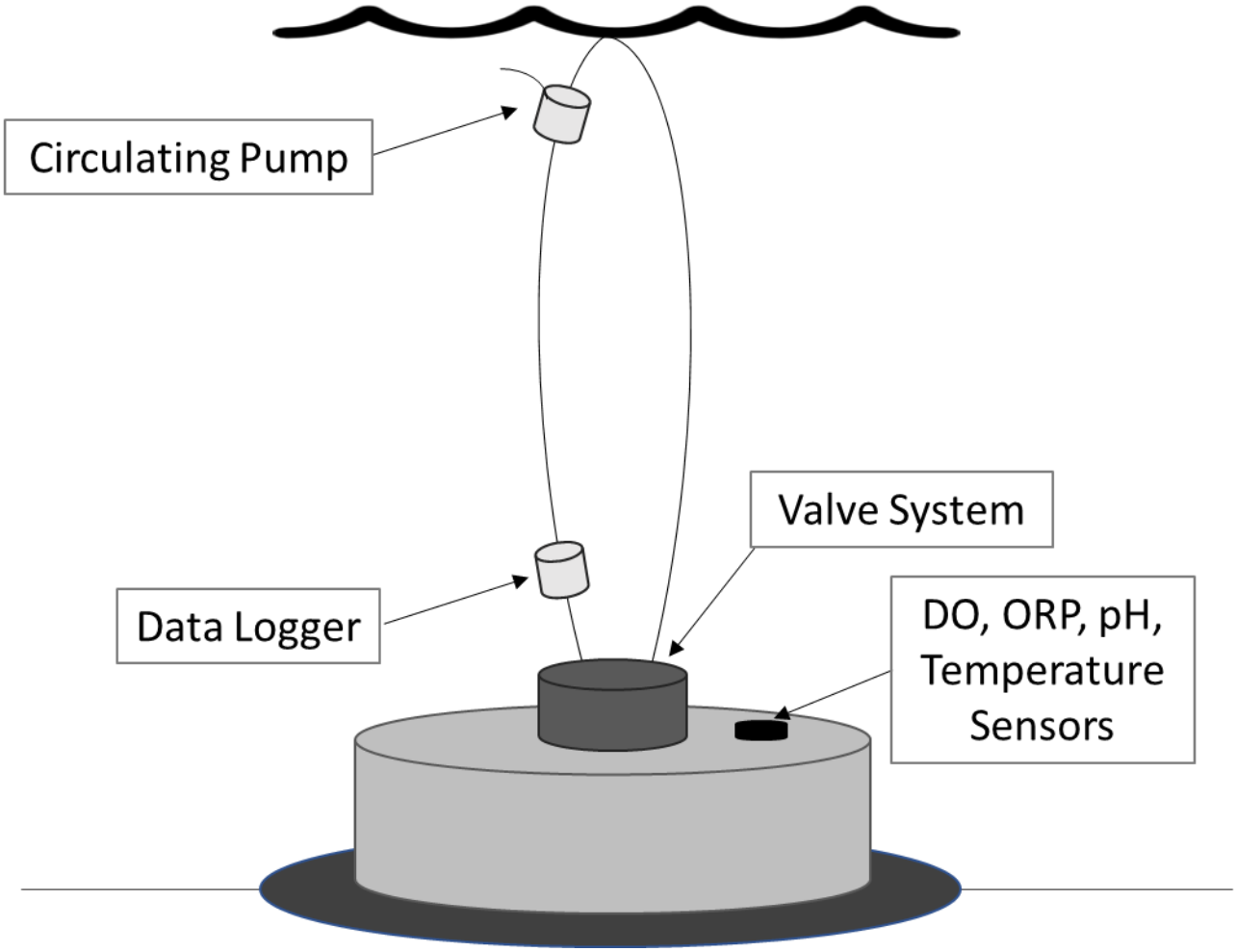


**Figure 4.** Conceptual drawing of key features of the flux chamber.

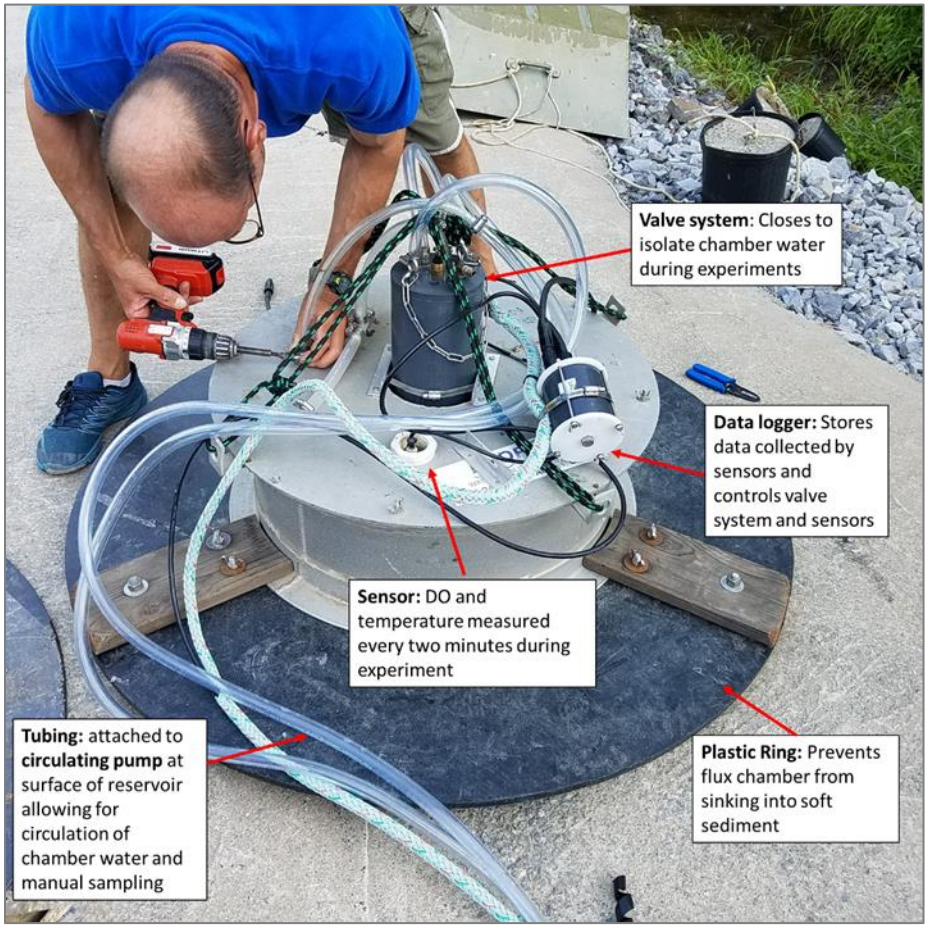


**Figure 5.** Picture showing preparation of the sediment flux chamber for deployment, with descriptions of the parts of the flux chambers.

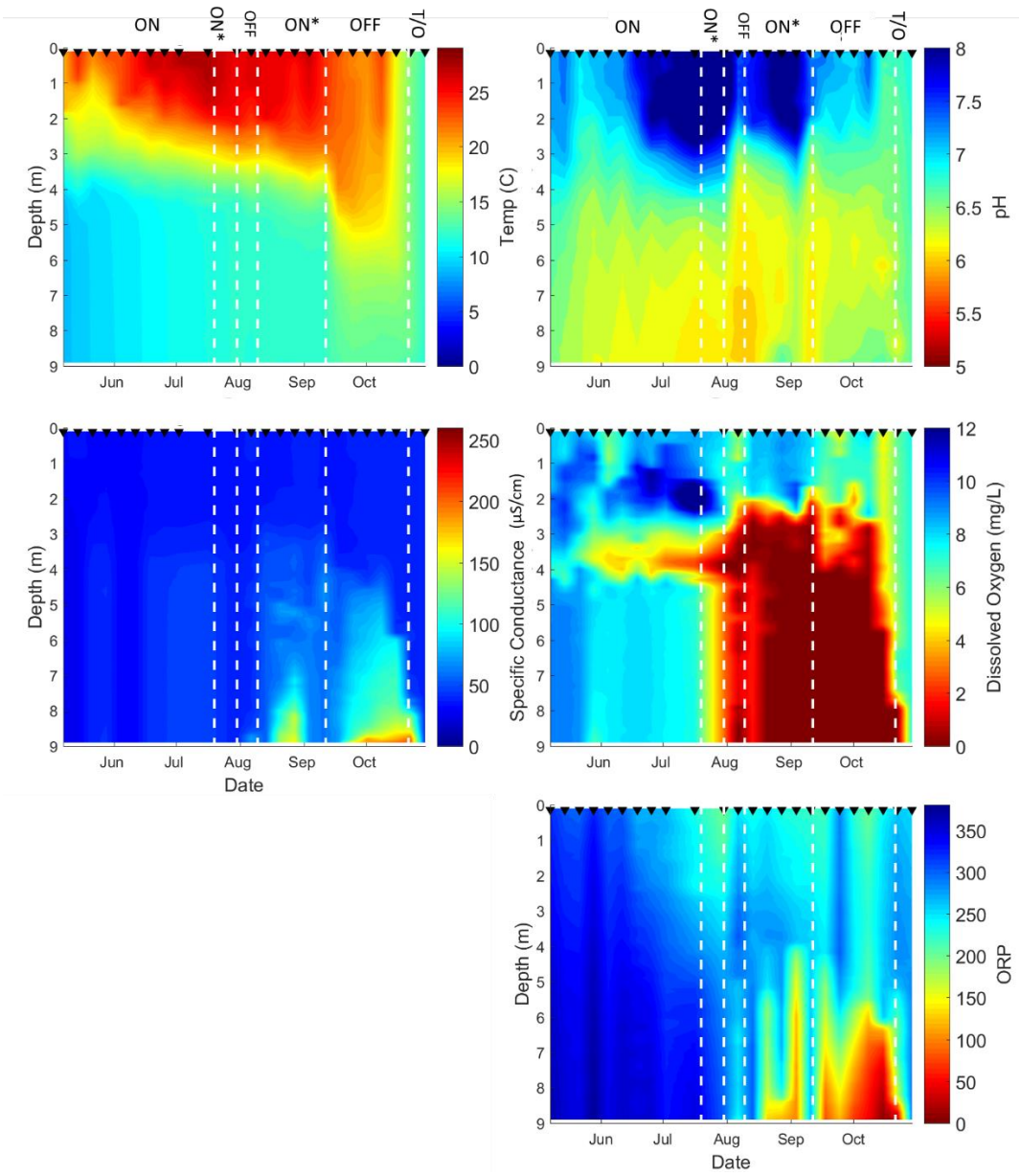


**Figure 6.** Dissolved oxygen concentrations (mg/L), temperature (C), pH, ORP (mV), and specific conductance (µS/cm) in FCR in 2018. Color scale on right shows concentrations. Dates of sampling shown as black triangles on top of figure. Between sampling dates, concentrations were linearly interpolated. White dashed lines show HOx system operation, including fully operational (ON), malfunctioning (ON*), and HOx system was not operational (OFF; see Table 1 for details).

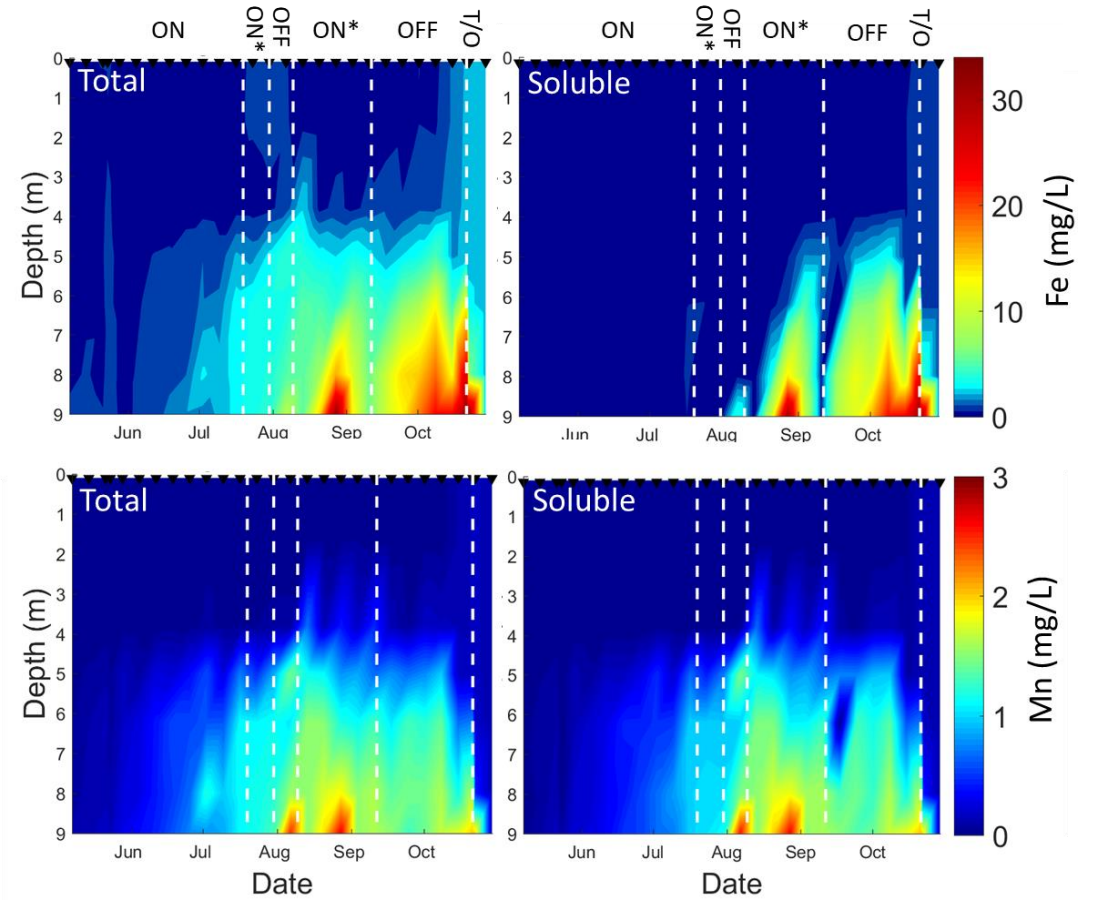


**Figure 7.** Soluble (right) and total (left) metal concentrations in FCR in 2018. Color scale on right shows concentrations. Dates of sampling shown as black triangles on top of figure. Between sampling dates, concentrations were linearly interpolated. White dashed lines show HOx system operation, including fully operational (ON), malfunctioning (ON*), and HOx system was not operational (OFF; see Table 1 for details).

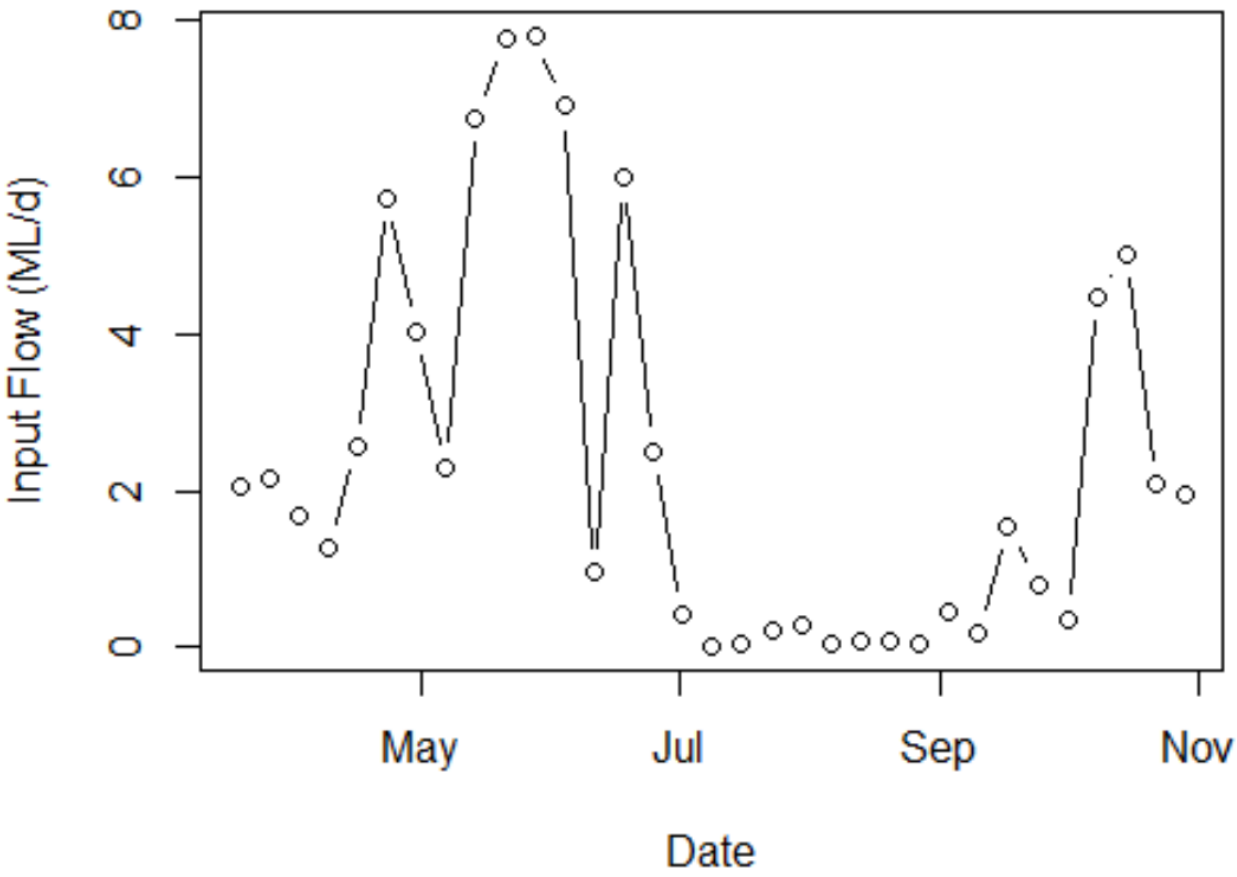


**Figure 8.** Averaged tributary inflow to FCR. A pressure sensor recorded water level at inflow every 15 minutes. This level was converted to a flow rate (mega liters (ML)/day; Eq 2) and averaged to a weekly time step.

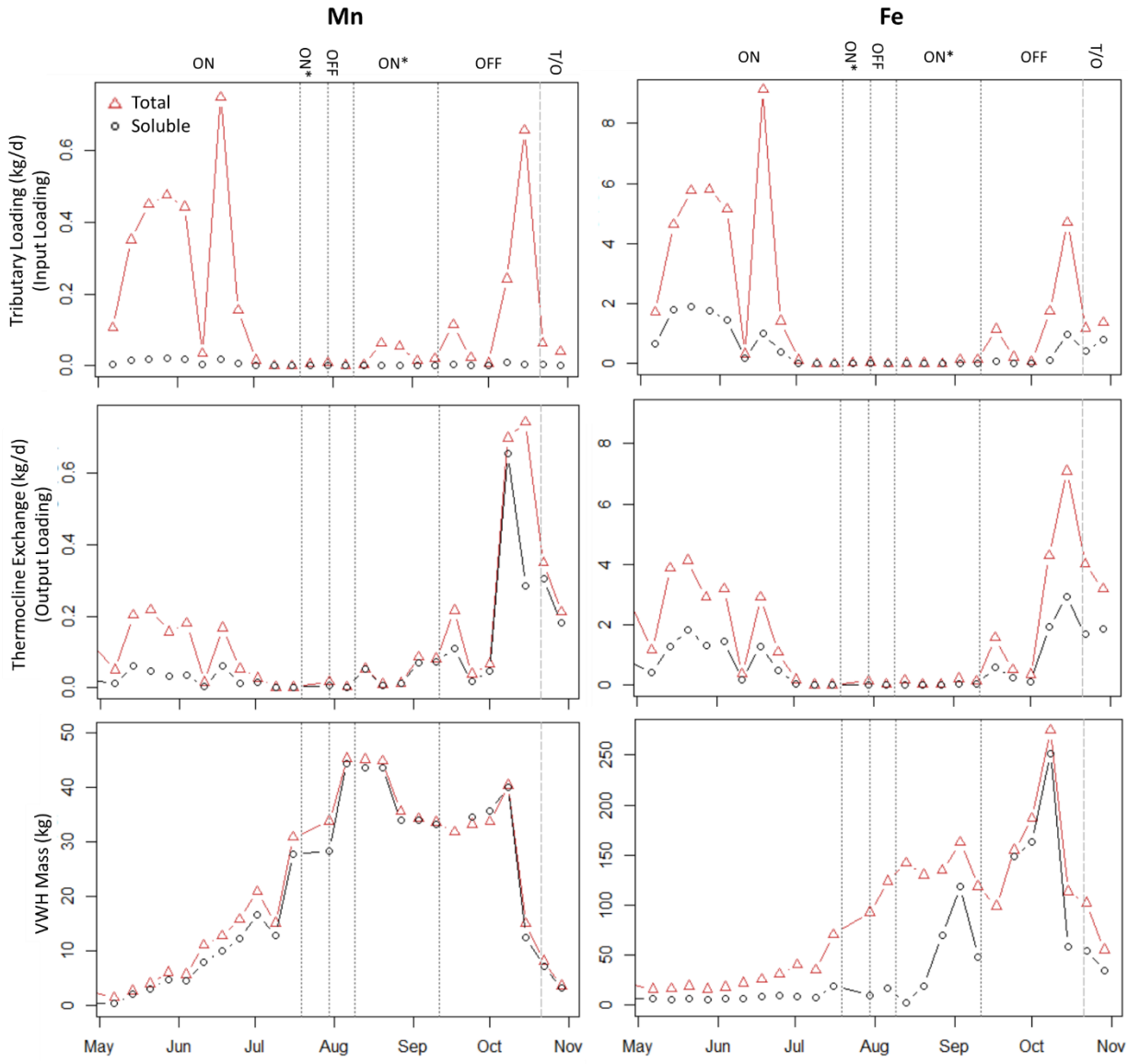


**Figure 9.** Total (red open triangles) and soluble (black open circles) Fe and Mn loading via the tributary (top), export via thermocline exchange (middle) and volume weighted hypolimnetic (VWH) mass (bottom). Dashed lines indicate HOx operation (see Table 1 for details) and turnover (T/O). White dashed lines show HOx system operation, including fully operational (ON), malfunctioning (ON*), and HOx system was not operational (OFF; see Table 1 for details).

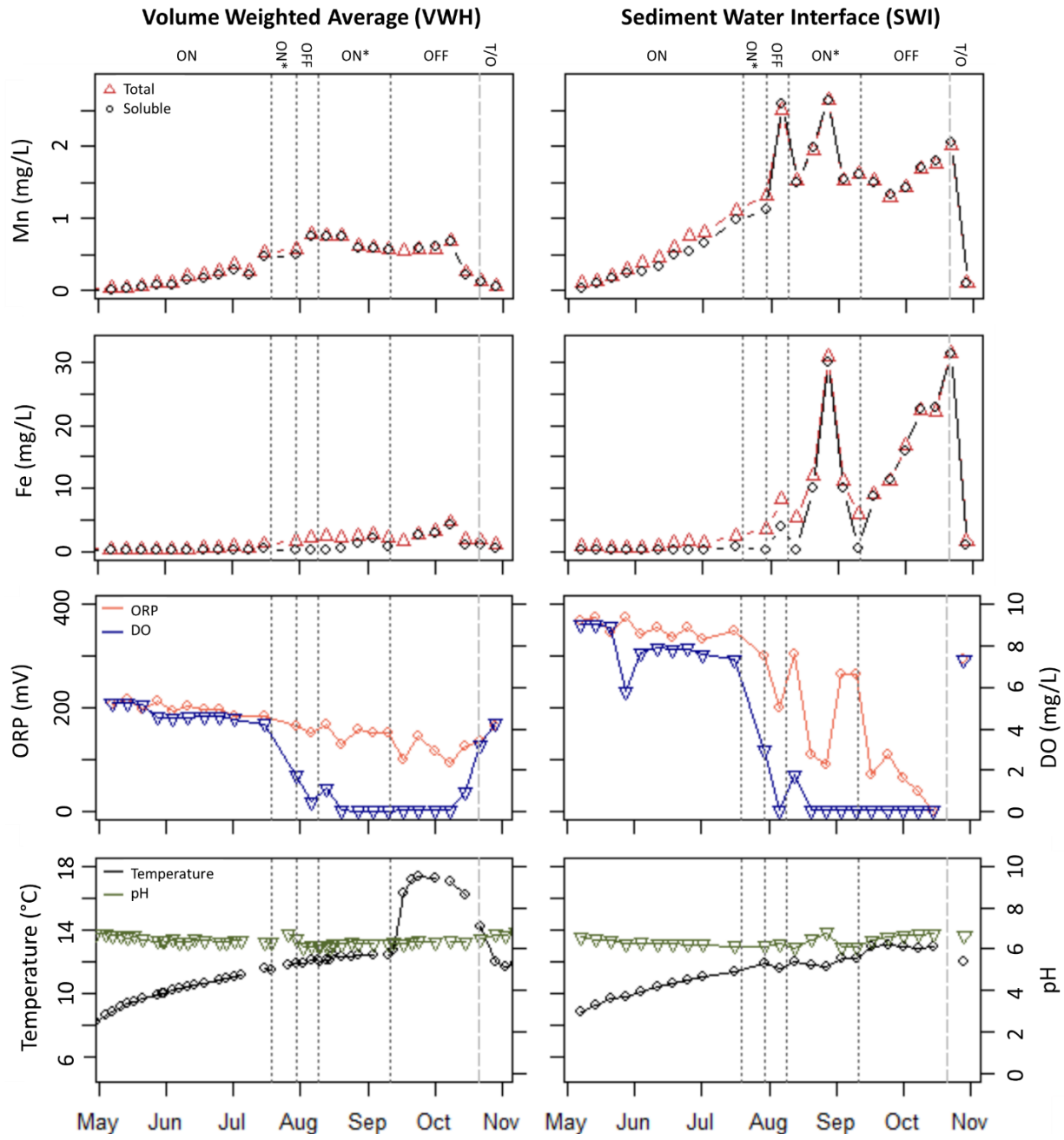


**Figure 10.** Total (red open triangle) and soluble (black open circle) Fe and Mn concentrations, ORP (coral), DO (blue), temperature (black bottom graphs) and pH (green) plotted at VWH concentrations (left) and at the SWI (9 m, right). Dashed lines show HOx system operation, including fully operational (ON), malfunctioning (ON*), and HOx system was not operational (OFF; see Table 1 for details).

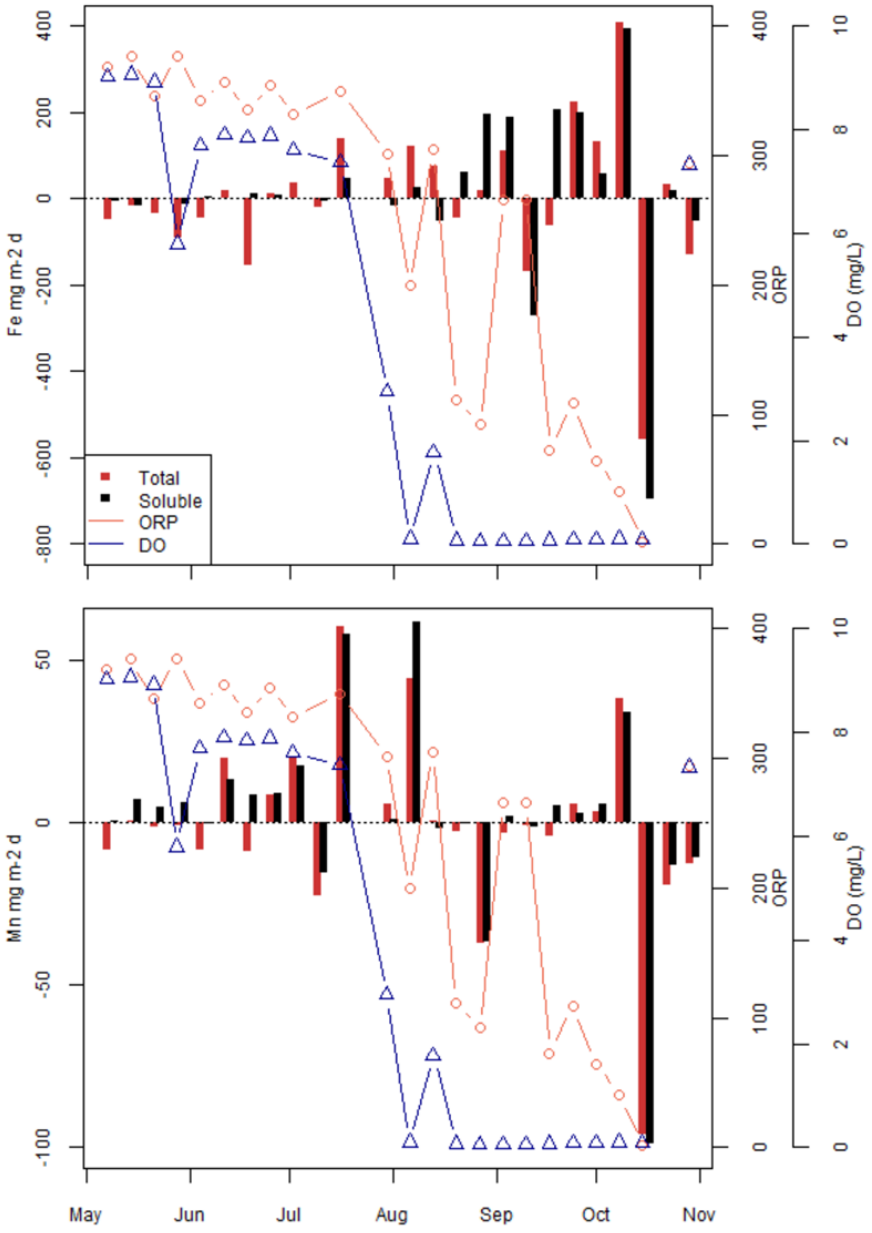


**Figure 11.** Total (red) and soluble (black) Fe (top) and Mn (bottom) fluxes calculated weekly using the hypolimnetic mass balance method. SWI ORP (orange) and DO (blue) were measured weekly.

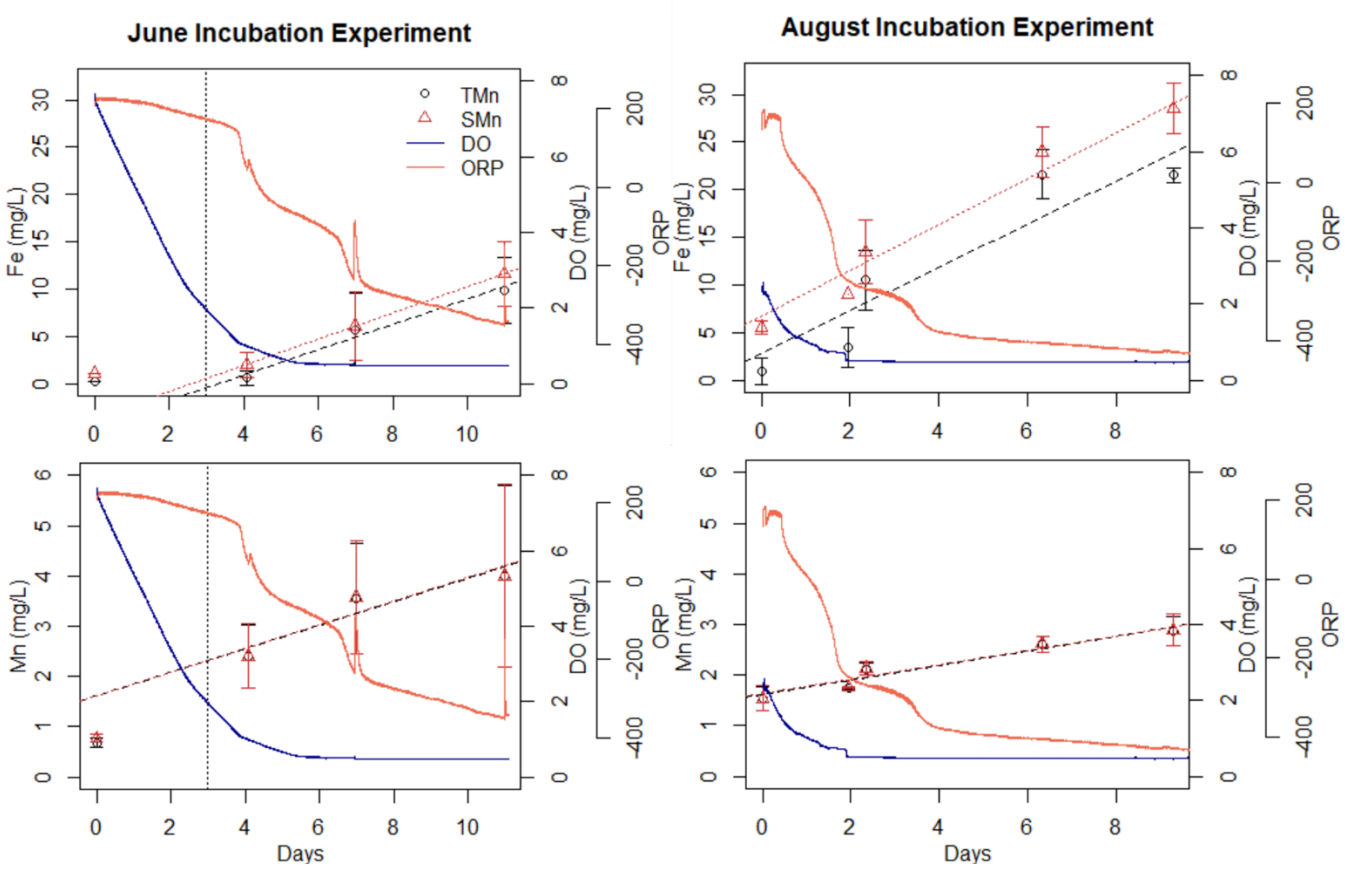


**Figure 12.** Results of June (6/21/2018-7/2/2018) and August (8/13/18-8/23/18) flux chamber experiments. Total (red open triangle) and soluble (black open circle) Fe and Mn concentrations shown over DO (blue) and ORP (orange). Average of the three flux chambers with one standard deviation plotted. Dashed line represents the beginning of the June experiments, where DO < 2 mg/L. The pH and temperature date are shown in the Appendix (Figure S7).

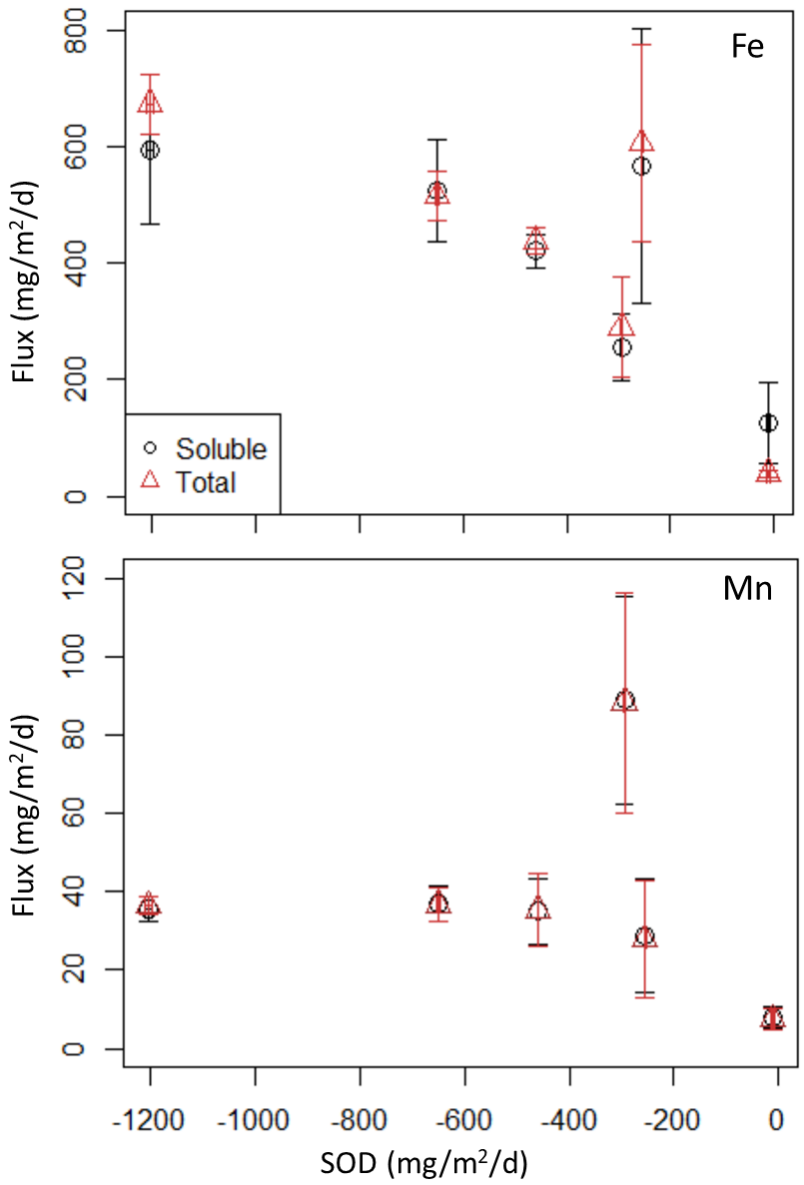


**Figure 13.** Results from the June, August, and water column flux chamber experiments: Total (red open triangle) and soluble (black open circle) Fe and Mn fluxes as function of Sediment Oxygen Demand (or negative DO flux). The flux value of each chamber is plotted with one standard deviation as error bars. Standard deviation of SOD was negligible.

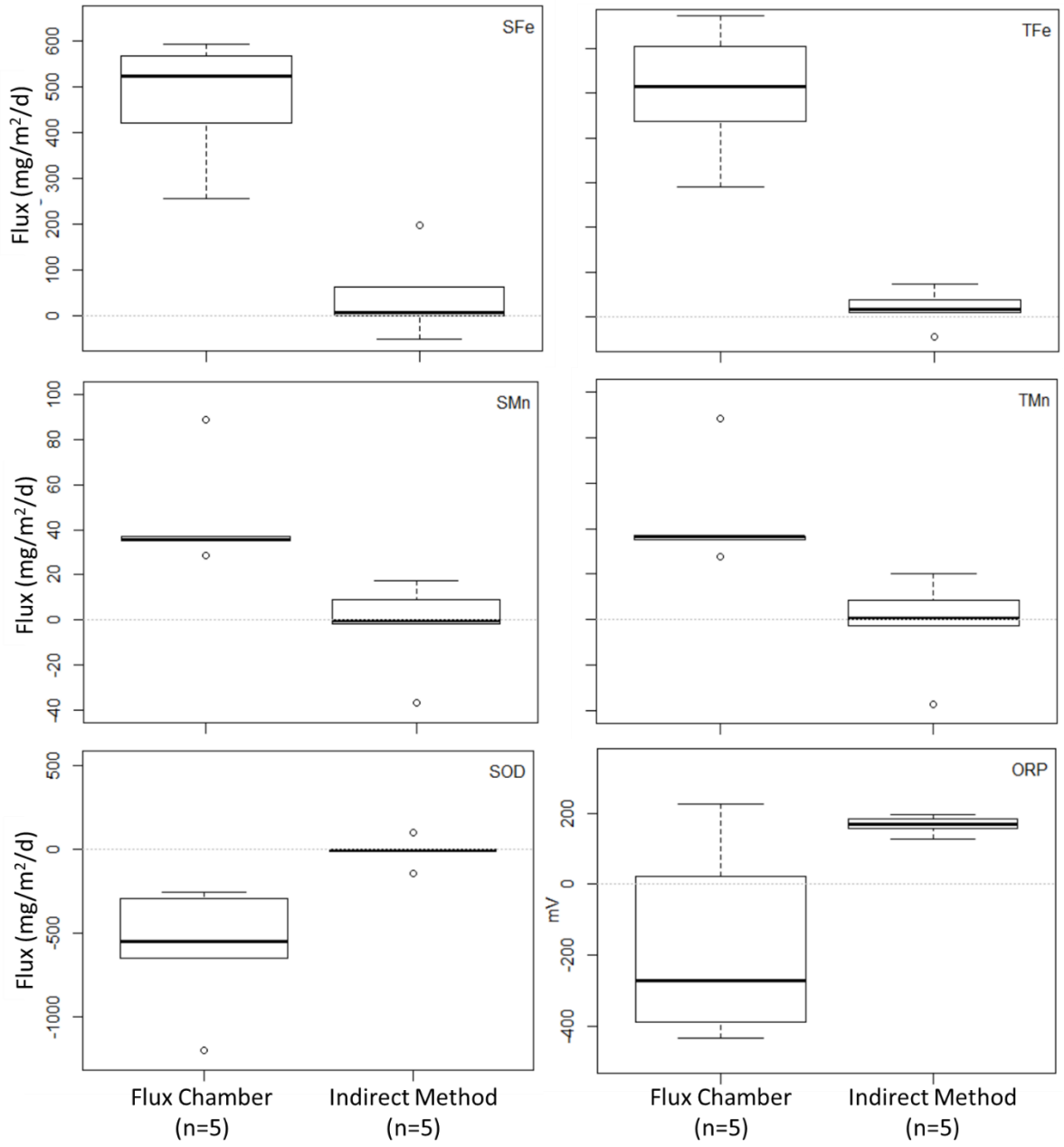


**Figure 14**. Box plots comparing all fluxes measured using the flux chamber method (n=5; both June and August experiments) and those estimates using the mass balance method during the same dates as the flux chamber experiment (n = 5).

**Table 1.** HOx operation dates in FCR. * Although the oxygen addition rate was reported at 22 and 19 kg/d, because the volume weighted hypolimnetic (VWH) DO never exceeded 2 mg/L during this time, we suspect that the oxygen system had malfunctioned.

| Date Range in 2018 | HOx System | Oxygen addition rate (kg/d) | Average VWH DO (mg/L) |
|---|---|---|---|
| Apr 24 – Jul 19 | ON | 16 | 4.7±0.3 |
| Jul 19 – Jul 30 | ON* | 22* | 1.8* |
| Jul 30 – Aug 9 | OFF | 0 | 0.5 |
| Aug 9 – Sep 11 | ON (partial*) | 19* | 0.3±0.5* |
| Sep 11-Oct 21 | OFF | 0 | 0.2±0.4 |
| Oct 21 | Turnover (TO) | N/A | N/A |

**Table 2.** Results of Wilcoxon rank sum test. The "June vs. August" experiment compares the June with the August flux chamber results. The "both" experiments compares the flux chamber results to the mass balance method results from the same dates as the chambers. Because the Wilcoxon test transforms raw data into ranks and the fluxes calculated in the direct vs. indirect method always had the same ranks regardless of their values, the statistics are identical.

| Metal | Experiment | Method | $\chi^2$ | p-value | DF |
|---|---|---|---|---|---|
| TFe | June vs. August | Flux Chamber | 3 | 0.08 | 1 |
| SFe | June vs. August | Flux Chamber | 3 | 0.08 | 1 |
| TMn | June vs. August | Flux Chamber | 0.3 | 0.56 | 1 |
| SMn | June vs. August | Flux Chamber | 0.3 | 0.56 | 1 |
| $O_2$ | June vs. August | Flux Chamber | 0.0 | 1 | 1 |
| TFe | Both | Both | 6.8 | 0.009 | 1 |
| SFe | Both | Both | 6.8 | 0.009 | 1 |
| TMn | Both | Both | 6.8 | 0.009 | 1 |
| SMn | Both | Both | 6.8 | 0.009 | 1 |

**Table 3.** Summary of sample data collected during flux chamber experiments. We also collected nitrogen, phosphorous, and greenhouse gas samples at the same times as the metals samples; data are not reported in this thesis. Replicate flux chambers are denoted A-C. ORP and pH were measured only in flux chamber B.

| Days | Flux Chamber | Experiment | Sample Number | SFe $\left(\frac{mg}{L}\right)$ | SMn $\left(\frac{mg}{L}\right)$ | TFe $\left(\frac{mg}{L}\right)$ | TMn $\left(\frac{mg}{L}\right)$ | DO $\left(\frac{mg}{L}\right)$ | Temp (°C) | ORP (mV) | pH |
|---|---|---|---|---|---|---|---|---|---|---|---|
| 0.0 | A | June | 0 | 0.3 | 0.7 | 1.1 | 0.8 | 7.4 | 13.8 | | |
| 4.1 | A | June | 1 | 0.2 | 2.7 | 1.1 | 2.7 | 1.8 | 12.7 | | |
| 7.1 | A | June | 2 | 1.8 | 4.4 | 2.4 | 4.5 | 0.5 | 12.5 | | |
| 11.0 | A | June | 3 | 7.4 | 5.3 | 9.2 | 5.3 | 0.5 | 12.5 | | |
| 0.0 | B | June | 0 | 0.3 | 0.6 | 1.1 | 0.7 | 8.1 | 13.2 | 216.0 | 6.3 |
| 4.1 | B | June | 1 | 0.2 | 1.7 | 1.5 | 1.7 | 0.6 | 12.5 | 52.0 | 6.3 |
| 7.0 | B | June | 2 | 5.9 | 2.3 | 6.1 | 2.3 | 0.5 | 12.7 | -135.0 | 6.7 |
| 11.0 | B | June | 3 | 12.3 | 2.7 | 14.0 | 2.7 | 0.5 | 12.6 | -349.0 | 7.0 |
| 0.0 | A | August | 0 | 0.1 | 1.4 | 5.4 | 1.4 | 0.5 | 14.5 | | |
| 1.0 | A | August | 2 | 13.1 | 2.2 | 16.3 | 2.3 | 0.5 | 13.6 | | |
| 5.0 | A | August | 3 | 21.3 | 2.5 | 24.1 | 2.5 | 0.4 | 13.6 | | |
| 8.0 | A | August | 4 | 21.5 | 2.6 | 28.0 | 2.6 | 0.4 | 13.6 | | |
| 0.0 | B | August | 0 | 0.1 | 1.4 | 4.9 | 1.4 | 2.3 | 14.3 | 177.0 | 6.4 |
| 2.0 | B | August | 1 | 4.9 | 1.7 | 9.1 | 1.7 | 0.5 | 13.6 | -248.0 | 6.7 |
| 3.0 | B | August | 2 | 11.5 | 2.0 | 14.3 | 2.0 | 0.5 | 13.7 | -284.0 | 7.0 |
| 7.0 | B | August | 3 | 24.3 | 2.6 | 26.6 | 2.6 | 0.5 | 13.8 | -411.0 | 7.3 |
| 9.9 | B | August | 4 | 22.3 | 2.9 | 31.4 | 2.9 | 0.5 | 13.5 | -434.0 | 7.5 |
| 0.0 | C | August | 0 | 2.5 | 1.8 | 6.3 | 1.8 | 2.7 | 14.2 | | |
| 1.9 | C | August | 1 | 1.9 | 1.7 | 9.1 | 1.8 | 0.6 | 13.8 | | |
| 3.0 | C | August | 2 | 7.0 | 2.1 | 9.8 | 2.1 | 0.6 | 13.3 | | |
| 7.0 | C | August | 3 | 19.2 | 2.8 | 21.2 | 2.8 | 0.6 | 14.0 | | |
| 9.9 | C | August | 4 | 20.8 | 3.2 | 26.2 | 3.2 | 0.6 | 13.6 | | |

**Table 4.** Comparison of fluxes from FCR to those of other studies

| Site | SMn $\left(\frac{mg}{\frac{m^2}{d}}\right)$ | TMn $\left(\frac{mg}{\frac{m^2}{d}}\right)$ | SFe $\left(\frac{mg}{\frac{m^2}{d}}\right)$ | TFe $\left(\frac{mg}{\frac{m^2}{d}}\right)$ | SOD $\left(\frac{mg}{\frac{m^2}{d}}\right)$ | Temp (°C) | Time of Year | Analysis Method | Location | Author |
|---|---|---|---|---|---|---|---|---|---|---|
| **Falling Creek Reservoir** | **34 (±2); 62 (±19)** | **34 (±2); 62 (±19)** | **338 (±58); 561 (±17)** | **364 (±52); 597 (±37)** | **467 (±101); 703 (±224.5)** | **11.5; 15** | **June/August** | **Flux Chamber** | **Vinton, VA, U.S.A.** | **This Study** |
| **Falling Creek Reservoir** | **-99-62** | **-96-61** | **-695-392** | **-559-408** | **-226-519** | **8.8-13** | **May - October** | **Metals Mass Balance** | **Vinton, VA, U.S.A.** | **This Study** |
| **Lake Bard** | | | | | 579 | 16 | | Experimental Incubation | Central Coast, CA, U.S.A. | (Beutel, 2003) |
| **Upper San Leandro Reservoir** | | | | | 450 | 16 | | Experimental Incubation | San Francisco Bay Area, CA, U.S.A. | (Beutel, 2003) |
| **Lake Sempach** | | | 45(±34)[a] 19(±17)[b] | | 82(±104)[a] 9(±4)[b] | | April - November | Flux Chamber[a]; Peeper[b] | Sempach, Switzerland | (Urban et al., 1997) |
| **Red Rock Reservoir; DeGray Reservoir** | | 39 (±5); 10 (±4) | | 66 (±15); 34 (±10) | | | | Experimental Incubation | Marion Co., IA; Clark Co., AR, U.S.A. | (Brannon et al., 1985) |
| **Lake Erie** | | | | | 300 | | Average of June - August | Flux Chamber | North America | (Adams et al., 1982) |
| **Rzeszow reservoir** | | | | | 460-730 | | Spring - Autumn | Flux Chamber | Rzeszow, Poland | (Tomaszek and Czerwieniec, 2000) |
| **Lake Bret** | 1[b], 7[c] | | 13[b], 20[c] | | | | July – October | Peepers[b]; Metals Mass Balance[c] | Vaud, Switzerland | (Belzile et al., 1996) |
| **Rostherne Mere** | 66-126 | | | ~0 | | 3-10 | June/October | Metals Mass Balance | Cheshire, England | (Davison and Woof, 1984) |
| **Esthwaite** | | | 10-190 | | | | | Metals Mass Balance | Lake District National Park | (Davison, 1993) |
| **Lake Fukami-ike** | 2 | | | | | | April - September | Metals Mass Balance | Central Japan | (Yagi, 1996) |
| **Carvins Cove Reservoir** | 19-37[b]; 77-857[d] | | | | 25.6(±40)-258(±37) | | June, August (a); May – October (b) | Peepers[b]; Voltammetric electrodes[d] | Roanoke, VA, U.S.A. | (Bryant et al., 2011a; Bryant et al., 2011b) |

## References


Adams, D. D., Matisoff, G., and Snodgrass, W. J., 1982, Flux of reduced chemical constituents (Fe2+, Mn2+, NHinf4sup+and CH4) and sediment oxygen demand in Lake Erie: Hydrobiologia, v. 91, no. 0, p. 405-414.

APHA, 1998, Standard methods for the examination of water and wastewater.

Belzile, N., Pizarro, J., Filella, M., and Buffle, J., 1996, Sediment diffusive fluxes of Fe, Mn, and P in a eutrophic lake: Contribution from lateral vs bottom sediments, 327-354 p.:

Berelson, W. M., and Hammond, D. E., 1986, The calibration of a new free-vehicle benthic flux chamber for use in the deep sea: Deep Sea Research Part A. Oceanographic Research Papers, v. 33, no. 10, p. 1439-1454.

Beutel, M. W., 2003, Hypolimnetic Anoxia and Sediment Oxygen Demand in California Drinking Water Reservoirs: Lake and Reservoir Management, v. 19, no. 3, p. 208-221.

Beutel, M. W., Leonard, T. M., Dent, S. R., and Moore, B. C., 2008, Effects of aerobic and anaerobic conditions on P, N, Fe, Mn, and Hg accumulation in waters overlaying profundal sediments of an oligo-mesotrophic lake: Water Research, v. 42, no. 8, p. 1953-1962.

Bouchard, M., Laforest, F., Vandelac, L., Bellinger, D., and Mergler, D., 2007, Hair Manganese and Hyperactive Behaviors: Pilot Study of School-Age Children Exposed through Tap Water: Environmental Health Perspectives, v. 115, no. 1, p. 122-127.

Bouchard, M. F., Sauvé, S., Barbeau, B., Legrand, M., Brodeur, M.-È., Bouffard, T., Limoges, E., Bellinger, D. C., and Mergler, D., 2011, Intellectual Impairment in School-Age Children Exposed to Manganese from Drinking Water: Environmental Health Perspectives, v. 119, no. 1, p. 138-143.

Brannon, J. M., Chen, R. L., and Gunnison, D., 1985, Sediment-water interactions and mineral cycling in reservoirs, *in* Gunnison, D., ed., Microbial Processes in Reservoirs: Dordrecht, Springer Netherlands, p. 121-134.

Bryant, L. D., Gantzer, P. A., and Little, J. C., 2011a, Increased sediment oxygen uptake caused by oxygenation-induced hypolimnetic mixing: Water Research, v. 45, no. 12, p. 3692-3703.

Bryant, L. D., Hsu-Kim, H., Gantzer, P. A., and Little, J. C., 2011b, Solving the problem at the source: Controlling Mn release at the sediment-water interface via hypolimnetic oxygenation: Water Research, v. 45, no. 19, p. 6381-6392.

Bryant, L. D., Little, J. C., and Bürgmann, H., 2012, Response of sediment microbial community structure in a freshwater reservoir to manipulations in oxygen availability: FEMS Microbiology Ecology, v. 80, no. 1, p. 248-263.

Bryant, L. D., Lorrai, C., McGinnis, D. F., Brand, A., est, A. W., and Little, J. C., 2010a, Variable sediment oxygen uptake in response to dynamic forcing: Limnology and Oceanography, v. 55, no. 2, p. 950-964.

Bryant, L. D., McGinnis, D. F., Lorrai, C., Brand, A., Little, J. C., and Wüest, A., 2010b, Evaluating oxygen fluxes using microprofiles from both sides of the sediment-water interface: Limnology and Oceanography: Methods, v. 8, no. 11, p. 610-627.

Carey, C. C., McClure, R. P., Gerling, A. B., Doubek, J. P., Chen, S., Lofton, M. E., and Hamre, K. D., 2019, Time series of high-frequency profiles of depth, temperature, dissolved oxygen, conductivity, specific conductivity, chlorophyll a, turbidity, pH, oxidation-reduction potential, photosynthetic active radiation, and descent rate for Beaverdam Reservoir, Carvins Cove Reservoir, Falling Creek Reservoir, Gatewood Reservoir, and Spring Hollow Reservoir in Southwestern Virginia, USA 2013-2018.: Environmental Data Initiative.

Carey, C. C., and Rydin, E., 2011, Lake trophic status can be determined by the depth distribution of sediment phosphorus: Limnology and Oceanography, v. 56, no. 6, p. 2051-2063.

Davison, W., 1981, Supply of iron and manganese to an anoxic lake basin: Nature, v. 290, no. 5803, p. 241-243.

Davison, W., 1993, Iron and manganese in lakes: Earth-Science Reviews, v. 34, no. 2, p. 119-163.

Davison, W., and Woof, C., 1984, A study of the cycling of manganese and other elements in a seasonally anoxic lake, Rostherne Mere, U.K: Water Research, v. 18, no. 6, p. 727-734.
Di Toro, D. M., and Connolly, J. P., 1980, Mathematical models of water quality in large lakes part 2: Lake Erie.
Du, J., 2004, Drinking Water Health Advisory for Manganese, *in* United States. Environmental Protection, A., ed.
Elrod, V. A., Berelson, W. M., Coale, K. H., and Johnson, K. S., 2004, The flux of iron from continental shelf sediments: A missing source for global budgets: Geophysical Research Letters, v. 31, no. 12.
Gantzer, P. A., Bryant, L. D., and Little, J. C., 2009, Controlling soluble iron and manganese in a water-supply reservoir using hypolimnetic oxygenation: Water Research, v. 43, no. 5, p. 1285-1294.
Gerling, A. B., Browne, R. G., Gantzer, P. A., Mobley, M. H., Little, J. C., and Carey, C. C., 2014, First report of the successful operation of a side stream supersaturation hypolimnetic oxygenation system in a eutrophic, shallow reservoir: Water Research, v. 67, p. 129-143.
Gerling, A. B., Munger, Z. W., Doubek, J. P., Hamre, K. D., Gantzer, P. A., Little, J. C., and Carey, C. C., 2016, Whole-Catchment Manipulations of Internal and External Loading Reveal the Sensitivity of a Century-Old Reservoir to Hypoxia: Ecosystems, v. 19, no. 3, p. 555-571.
Groschen, G. E., Arnold, T. L., Morrow, W. S., and Warner, K. L., 2009, Occurrence and distribution of iron, manganese, and selected trace elements in ground water in the glacial aquifer system of the Northern United States: U. S. Geological Survey.
Hicks, D., Environmental Protection Agency Region IV perspective on SOD, *in* Proceedings Proceedings: US Army Corps of Engineers workshop on sediment oxygen demand1990, p. 110-119.
Khan, K., Factor-Litvak, P., Wasserman, G. A., Liu, X., Ahmed, E., Parvez, F., Slavkovich, V., Levy, D., Mey, J., Geen, A. v., and Graziano, J. H., 2011, Manganese Exposure from Drinking Water and Children’s Classroom Behavior in Bangladesh: Environmental Health Perspectives, v. 119, no. 10, p. 1501-1506.
Langmuir, D., 1997, Aqueous Environmental Geochemistry, Prentice-Hall Inc. .
Madigan, M. T., Martinko, J. M., and Parker, J., 1997, Brock biology of microorganisms, Prentice hall Upper Saddle River, NJ.
McMahon, P. B., Belitz, K., Reddy, J. E., and Johnson, T. D., 2019, Elevated Manganese Concentrations in United States Groundwater, Role of Land Surface–Soil–Aquifer Connections: Environmental Science & Technology, v. 53, no. 1, p. 29-38.
Munger, Z. W., Carey, C. C., Gerling, A. B., Hamre, K. D., Doubek, J. P., Klepatzki, S. D., McClure, R. P., and Schreiber, M. E., 2016, Effectiveness of hypolimnetic oxygenation for preventing accumulation of Fe and Mn in a drinking water reservoir: Water Research, v. 106, no. Supplement C, p. 1-14.
Oulhote, Y., Mergler, D., Barbeau, B., Bellinger, D. C., Bouffard, T., Brodeur, M.-È., Saint-Amour, D., Legrand, M., Sauvé, S., and Bouchard, M. F., 2014, Neurobehavioral Function in School-Age Children Exposed to Manganese in Drinking Water: Environmental Health Perspectives, v. 122, no. 12, p. 1343-1350.
Pais, I., and Jones, J. B., 1997, The Handbook of Trace Elements, Taylor & Francis.
Pakhomova, S. V., Hall, P. O. J., Kononets, M. Y., Rozanov, A. G., Tengberg, A., and Vershinin, A. V., 2007, Fluxes of iron and manganese across the sediment–water interface under various redox conditions: Marine Chemistry, v. 107, no. 3, p. 319-331.
Polak, J., and Haffner, D., 1978, Oxygen depletion of Hamilton Harbour: Water Research, v. 12, no. 4, p. 205-215.
Read, J. S., Hamilton, D. P., Jones, I. D., Muraoka, K., Winslow, L. A., Kroiss, R., Wu, C. H., and Gaiser, E., 2011, Derivation of lake mixing and stratification indices from high-resolution lake buoy data: Environmental Modelling & Software, v. 26, no. 11, p. 1325-1336.
Steefel, C. I., DePaolo, D. J., and Lichtner, P. C., 2005, Reactive transport modeling: An essential tool and a new research approach for the Earth sciences: Earth and Planetary Science Letters, v. 240, no. 3, p. 539-558.

Teasdale, P. R., Batley, G. E., Apte, S. C., and Webster, I. T., 1995, Pore water sampling with sediment peepers: TrAC Trends in Analytical Chemistry, v. 14, no. 6, p. 250-256.

Tengberg, A., Hall, P. O. J., Andersson, U., Lindén, B., Styrenius, O., Boland, G., de Bovee, F., Carlsson, B., Ceradini, S., Devol, A., Duineveld, G., Friemann, J. U., Glud, R. N., Khripounoff, A., Leather, J., Linke, P., Lund-Hansen, L., Rowe, G., Santschi, P., de Wilde, P., and Witte, U., 2005, Intercalibration of benthic flux chambers: II. Hydrodynamic characterization and flux comparisons of 14 different designs: Marine Chemistry, v. 94, no. 1, p. 147-173.

Tomaszek, J. A., and Czerwieniec, E., 2000, In situ chamber denitrification measurements in reservoir sediments: an example from southeast Poland: Ecological Engineering, v. 16, no. 1, p. 61-71.

Urban, N. R., Dinkel, C., and Wehrli, B., 1997, Solute transfer across the sediment surface of a eutrophic lake: I. Porewater profiles from dialysis samplers: Aquatic Sciences, v. 59, no. 1, p. 1-25.

USEPA, 2017, Secondary Drinking Water Standards: Guidance for Nuisance Chemicals.

Walker, R. R., and Snodgrass, W. J., 1986, Model for Sediment Oxygen Demand in Lakes: Journal of Environmental Engineering, v. 112, no. 1, p. 25-43.

Wasserman, G. A., Liu, X., Parvez, F., Factor-Litvak, P., Ahsan, H., Levy, D., Kline, J., van Geen, A., Mey, J., Slavkovich, V., Siddique, A. B., Islam, T., and Graziano, J. H., 2011, Arsenic and manganese exposure and children's intellectual function: Neurotoxicology, v. 32, no. 4, p. 450-457.

Woodward, H. P., 1932, Geology and Mineral Resources of the Roanoke Area, Virginia, *in* Survey, V. G., ed.

World Health Organization, 1996, Iron in drinking-water: background document for development of WHO guidelines for drinking-water quality.

-, 2004, Manganese in drinking-water: background document for development of WHO guidelines for drinking-water quality.

Yagi, A., 1996, Manganese flux associated with dissolved and suspended manganese forms in Lake Fukami-ike: Water Research, v. 30, no. 8, p. 1823-1832.

## Appendix

### A. Additional flux chamber experiments

In addition to the ten-day experiments, we conducted several other short-term experiments with the flux chambers. In mid-June 2018, we ran 3 three-hour experiments at high initial DO concentrations (6-8 mg/L) to examine metal fluxes across the SWI under oxic conditions. During the experiment, DO decreased <1 mg/L, supporting the maintenance of high DO during the experiment period. Metal samples were collected every 45 minutes. In late August 2018, we also conducted a pH manipulation experiment to evaluate if increasing the pH under oxic conditions would enhance Mn oxidation, as has been shown in laboratory studies. For this experiment, we filled one chamber with a mix of epilimnetic and hypolimnetic water to achieve an initial DO of 5 mg/L and a pH of 6.7. We collected samples to get baseline Fe and Mn concentrations. Using syringes attached to the inlet port, we injected a total of 5g of Na2CO3, increasing the pH in the chamber to 10.05. Metal samples were collected every 15 minutes for a total of 4 hours.

For the high DO experiment, DO was between 6-8 mg/L (Figure S2) during the experiments, and no detectable total Fe fluxes. Results for soluble Fe and total and soluble Mn was mixed, in one experiments, there was no detectable soluble or total Mn, but there was a significant soluble Fe flux of 0.66±0.22 mg/L/d and for the other experiment, total and soluble Mn had significant fluxes of 0.48±0.05 mg/L/d and 0.71±0.15 mg/L/d respectively (Figure S1).

For the pH experiment, pH was manipulated by adding sodium carbonate (Figure S3). Initial pH of both chambers was 6.76 and final pH was 10.25. Total and soluble Fe increased 16.72±2.66 mg/L/d and 9.98 ±0.525 mg/L/d. Total and soluble Mn returned to the sediments with -0.759±0.17 mg/L/d and -1.74±0.5714 mg/L/d (Figure S3). DO during the experiment remained constant at approximately 5 mg/L.

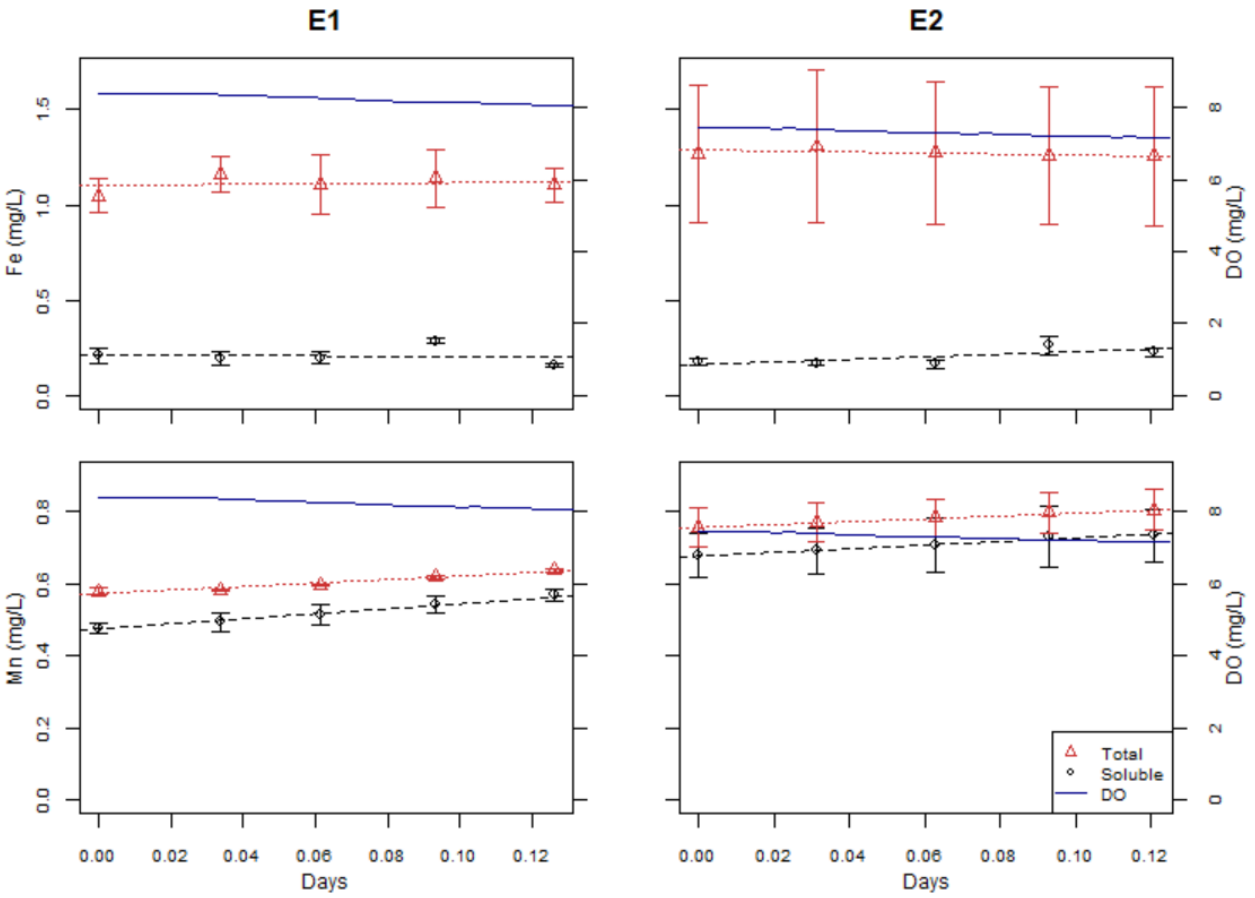


**Figure S1.** Total (red) and soluble (black) concentrations plotted with 1 standard deviation as error bars. Experiments 1 and 2 were done in early June over 4 hour period with DO > 6 mg/L

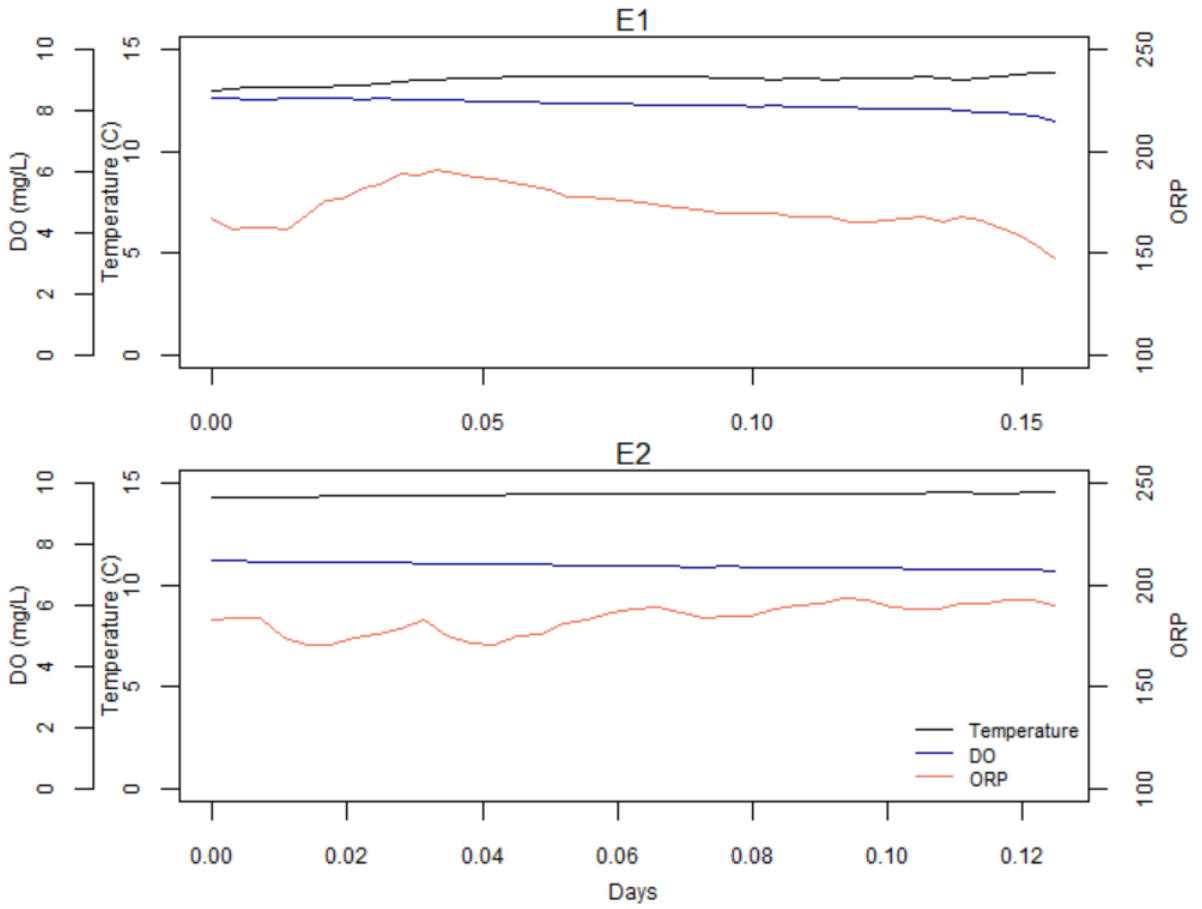


**Figure S2.** Temperature (black), DO (blue), and ORP (coral). Experiments 1 and 2 were done in early June over 4 hour period with DO > 6 mg/L

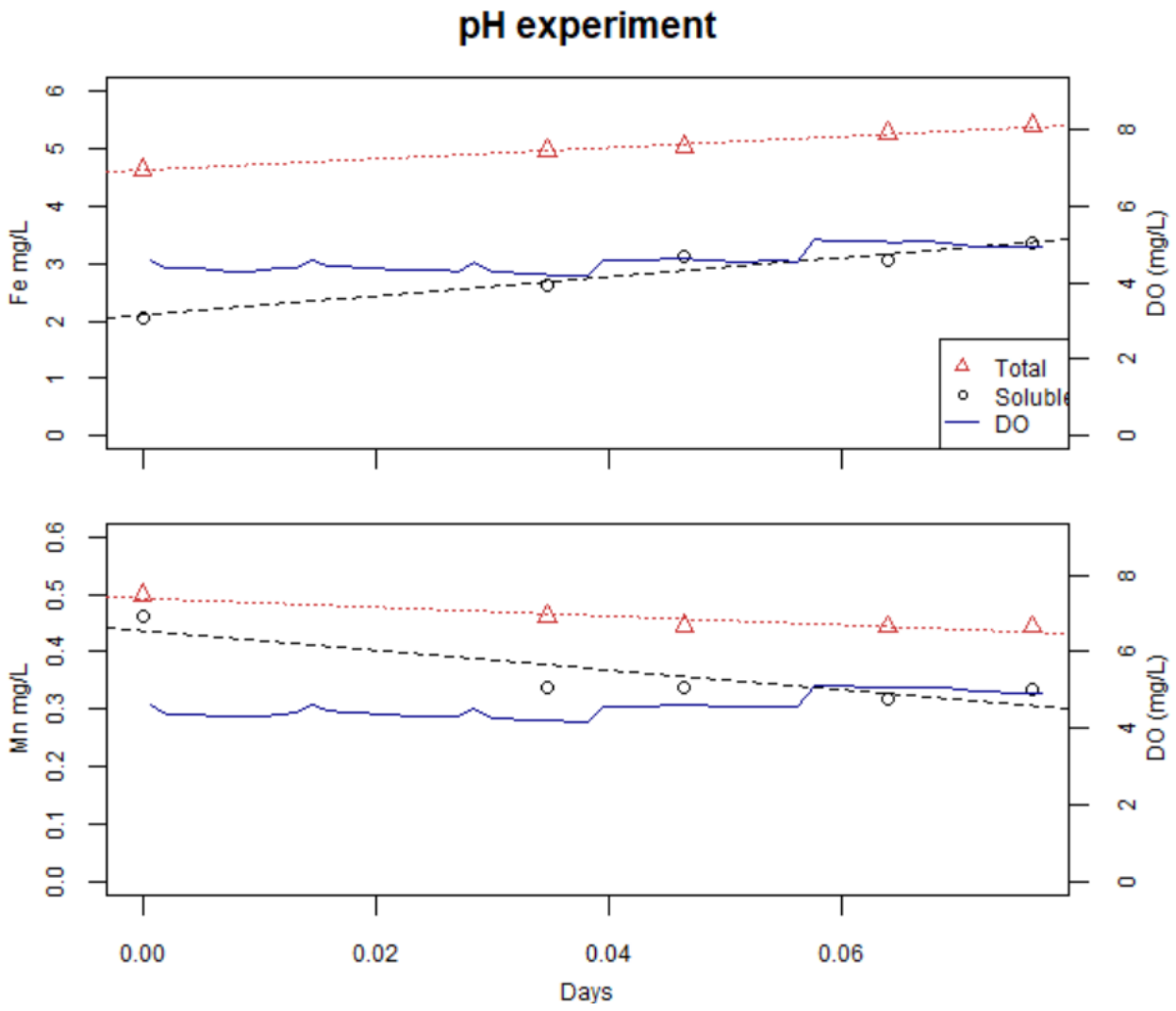


**Figure S3.** Total (red) and soluble (black) concentrations plotted. Experiment was run over 3 hours

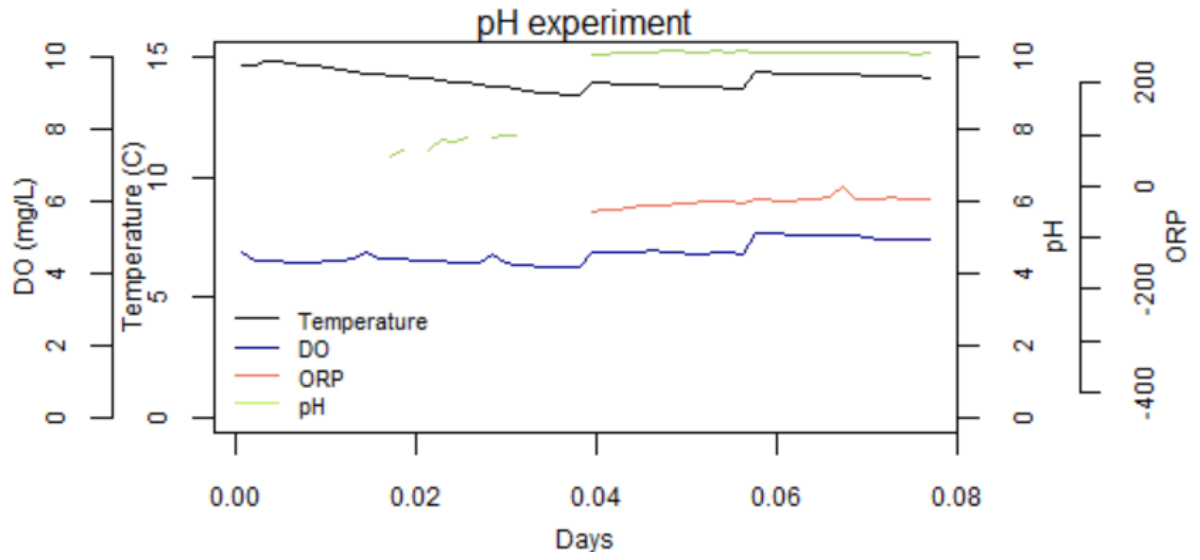


**Figure S4.** Temperature (black), DO (blue), and ORP (coral). Experiment run in mid-August for 3 days.

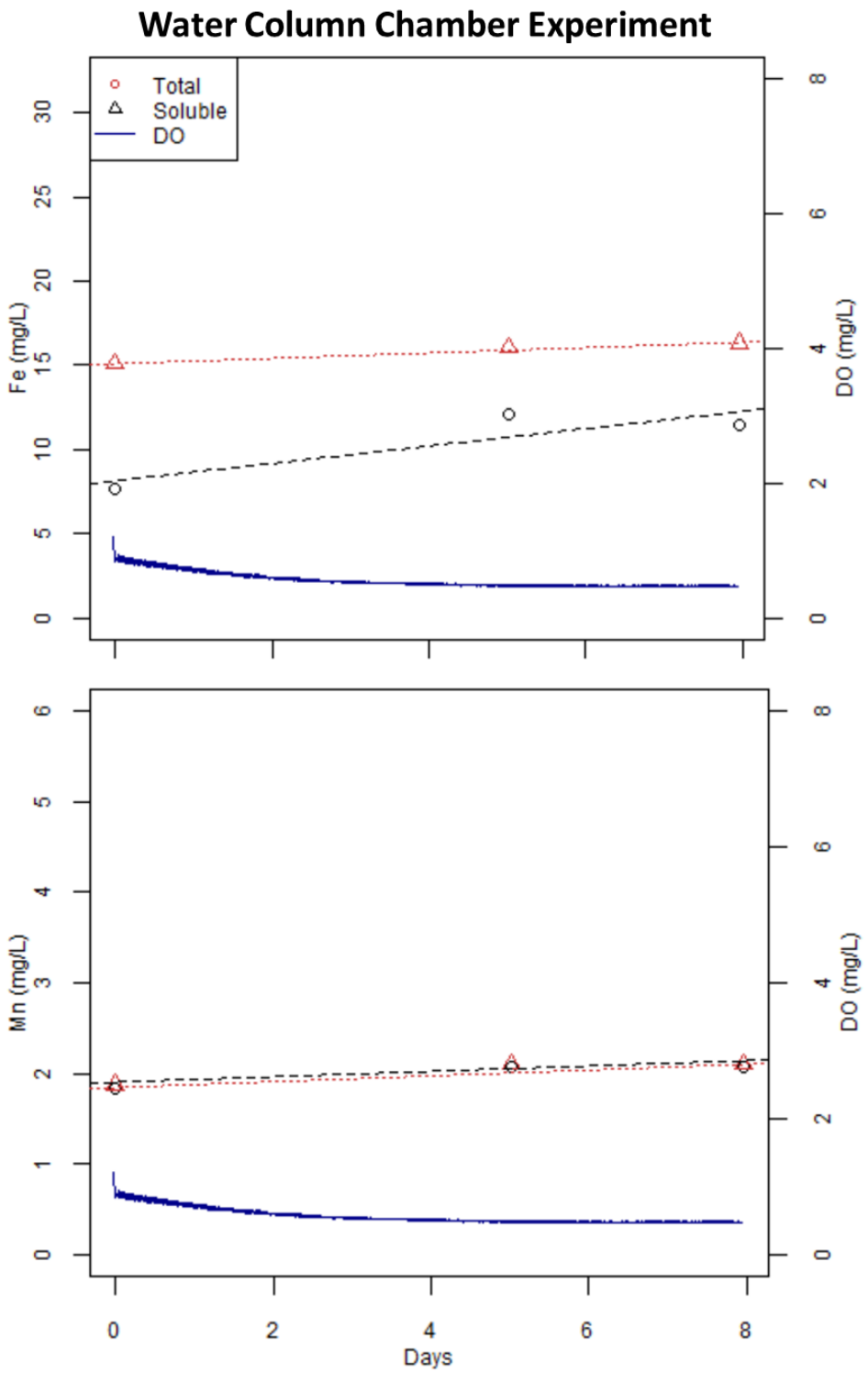


**Figure S6.** Results of August (8/13/18-8/23/18) water column chamber experiment. Total (red open triangle), soluble (black open circle) metals and DO (blue) are plotted. Dashed lines show line of best fit (slope not statistically different than 0; $p>0.05$)

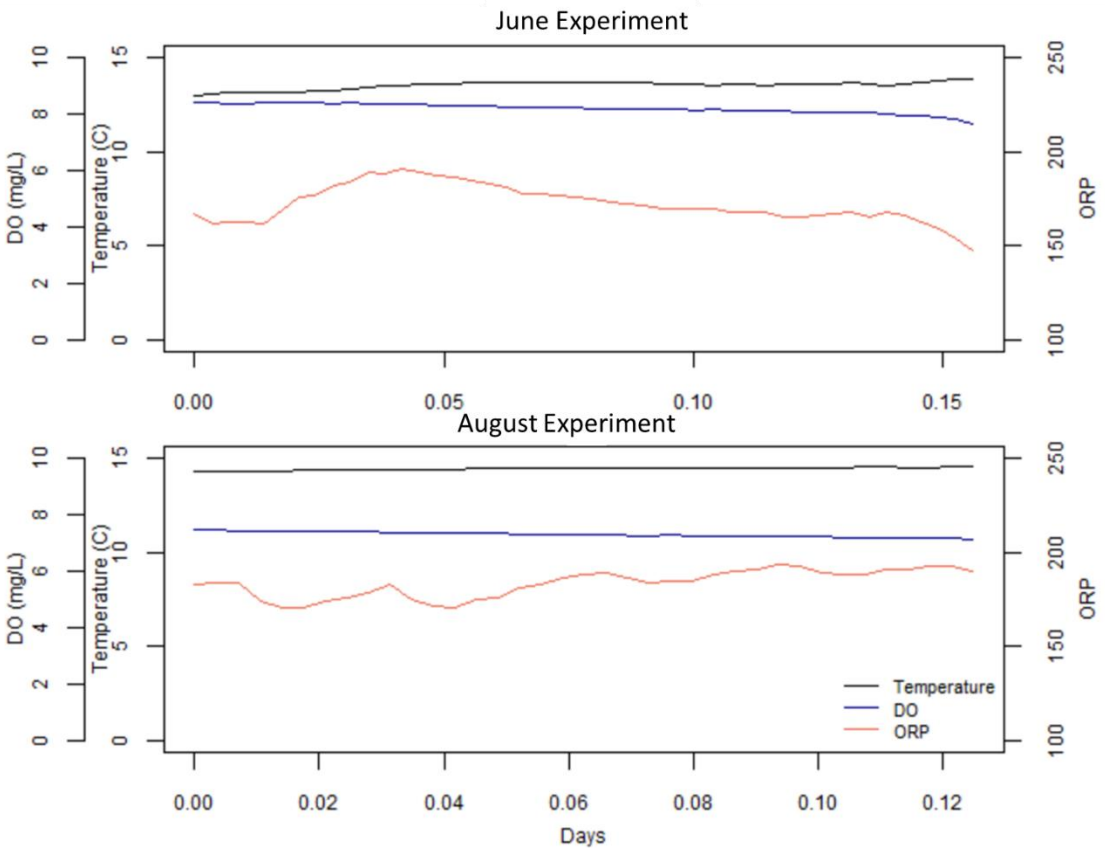


**Figure S7.** pH, ORP, and temperature changes in the flux chamber experiments.

**Table S1.** Summary of Sediment Water Interface Concentrations of metals and chemistry data.

| Date | TFe $\left(\frac{mg}{L}\right)$ | TMn $\left(\frac{mg}{L}\right)$ | SFe $\left(\frac{mg}{L}\right)$ | SMn $\left(\frac{mg}{L}\right)$ | Temp (°C) | DO $\left(\frac{mg}{L}\right)$ | pH | ORP (mV) | Inflow (ML/d) |
|---|---|---|---|---|---|---|---|---|---|
| 5/7/2018 | 0.8 | 0.1 | 0.2 | 0.0 | 8.8 | 9.0 | 6.6 | 368.0 | 2289751.9 |
| 5/14/2018 | 0.8 | 0.1 | 0.2 | 0.1 | 9.3 | 9.1 | 6.5 | 376.2 | 6760339.1 |
| 5/21/2018 | 0.6 | 0.2 | 0.2 | 0.2 | 9.6 | 8.9 | 6.4 | 345.5 | 7770015.7 |
| 5/28/2018 | 0.5 | 0.3 | 0.2 | 0.2 | 9.8 | 5.8 | 6.3 | 376.8 | 7806624.0 |
| 6/4/2018 | 0.6 | 0.4 | 0.2 | 0.2 | 10.1 | 7.7 | 6.3 | 342.9 | 6914765.5 |
| 6/11/2018 | 0.7 | 0.4 | 0.2 | 0.3 | 10.4 | 7.9 | 6.3 | 356.9 | 949120.1 |
| 6/18/2018 | 1.3 | 0.6 | 0.2 | 0.5 | 10.6 | 7.8 | 6.3 | 335.5 | 5992555.4 |
| 6/25/2018 | 1.6 | 0.8 | 0.2 | 0.5 | 10.9 | 7.9 | 6.2 | 354.4 | 2501559.9 |
| 7/2/2018 | 1.4 | 0.8 | 0.3 | 0.7 | 11.0 | 7.6 | 6.2 | 331.8 | 419707.0 |
| 7/9/2018 | 2.5 | 1.1 | 0.6 | 1.0 | | | | | 28285.5 |
| 7/16/2018 | 3.5 | 1.3 | 0.2 | 1.1 | 11.4 | 7.4 | 6.1 | 349.5 | 31391.6 |
| 7/30/2018 | 8.3 | 2.5 | 4.0 | 2.6 | 11.9 | 3.0 | 6.1 | 301.6 | 273076.0 |
| 8/6/2018 | 5.2 | 1.5 | 0.2 | 1.5 | 11.6 | 0.1 | 6.2 | 199.6 | 37194.1 |
| 8/13/2018 | 12.1 | 1.9 | 10.0 | 2.0 | 12.0 | 1.8 | 6.1 | 304.6 | 77052.7 |
| 8/20/2018 | 30.9 | 2.7 | 30.1 | 2.6 | 11.8 | 0.1 | 6.5 | 111.3 | 71276.2 |
| 8/27/2018 | 11.1 | 1.5 | 10.1 | 1.5 | 11.7 | 0.1 | 6.8 | 91.9 | 30416.7 |
| 9/3/2018 | 5.8 | 1.6 | 0.6 | 1.6 | 12.3 | 0.1 | 6.1 | 265.9 | 462049.6 |
| 9/10/2018 | 9.0 | 1.5 | 8.7 | 1.5 | 12.3 | 0.1 | 6.1 | 265.9 | 176989.2 |
| 9/17/2018 | 11.1 | 1.3 | 11.4 | 1.3 | 12.9 | 0.1 | 6.4 | 72.6 | 1556999.2 |
| 9/24/2018 | 16.8 | 1.4 | 15.9 | 1.4 | 13.0 | 0.1 | 6.6 | 109.4 | 811610.9 |
| 10/1/2018 | 22.3 | 1.7 | 22.5 | 1.7 | 12.9 | 0.1 | 6.7 | 64.5 | 354486.0 |
| 10/8/2018 | 22.2 | 1.8 | 22.9 | 1.8 | 12.9 | 0.1 | 6.7 | 40.7 | 4476633.4 |
| 10/15/2018 | 31.4 | 2.0 | 31.3 | 2.0 | 13.0 | 0.1 | 6.8 | 1.4 | 5015703.2 |
| 10/22/2018 | 1.6 | 0.1 | 1.0 | 0.1 | | | | | 2077532.1 |
| 10/29/2018 | 0.8 | 0.1 | 0.2 | 0.0 | 12.0 | 7.3 | 6.6 | 294.7 | 1955844.4 |

**Table S2.** Volume Weighted Metals and chemistry data for FCR for the 2018 season.

| Date | TFe $\left(\frac{mg}{L}\right)$ | SFe $\left(\frac{mg}{L}\right)$ | TMn $\left(\frac{mg}{L}\right)$ | SMn $\left(\frac{mg}{L}\right)$ | DO $\left(\frac{mg}{L}\right)$ | ORP (mV) | Temp (°C) | pH |
|---|---|---|---|---|---|---|---|---|
| 5/7/2018 | 0.3 | 0.1 | 0.0 | 0.0 | 5.2 | 209.0 | 8.8 | 6.7 |
| 5/14/2018 | 0.3 | 0.1 | 0.0 | 0.0 | 5.3 | 216.2 | 9.4 | 6.5 |
| 5/21/2018 | 0.3 | 0.1 | 0.1 | 0.1 | 5.1 | 197.1 | 9.7 | 6.5 |
| 5/28/2018 | 0.3 | 0.1 | 0.1 | 0.1 | 4.6 | 213.6 | 9.9 | 6.4 |
| 6/4/2018 | 0.3 | 0.1 | 0.1 | 0.1 | 4.5 | 195.0 | 10.2 | 6.5 |
| 6/11/2018 | 0.4 | 0.1 | 0.2 | 0.1 | 4.6 | 203.3 | 10.4 | 6.4 |
| 6/18/2018 | 0.4 | 0.1 | 0.2 | 0.2 | 4.6 | 198.0 | 10.7 | 6.4 |
| 6/25/2018 | 0.5 | 0.2 | 0.3 | 0.2 | 4.6 | 196.6 | 10.9 | 6.4 |
| 7/2/2018 | 0.7 | 0.2 | 0.4 | 0.3 | 4.5 | 183.5 | 11.1 | 6.4 |
| 7/9/2018 | 0.6 | 0.1 | 0.3 | 0.2 | | | | |
| 7/16/2018 | 1.2 | 0.3 | 0.5 | 0.5 | 4.2 | 184.9 | 11.5 | 6.3 |
| 7/30/2018 | 1.6 | 0.2 | 0.6 | 0.5 | 1.8 | 164.1 | 11.9 | 6.5 |
| 8/6/2018 | 2.1 | 0.3 | 0.8 | 0.8 | 0.5 | 152.3 | 12.1 | 6.2 |
| 8/13/2018 | 2.4 | 0.0 | 0.8 | 0.7 | 1.1 | 168.4 | 12.1 | 6.2 |
| 8/20/2018 | 2.2 | 0.3 | 0.8 | 0.7 | 0.1 | 128.7 | 12.3 | 6.3 |
| 8/27/2018 | 2.3 | 1.2 | 0.6 | 0.6 | 0.0 | 157.7 | 12.4 | 6.3 |
| 9/3/2018 | 2.8 | 2.0 | 0.6 | 0.6 | 0.0 | 152.0 | 12.4 | 6.2 |
| 9/10/2018 | 2.0 | 0.8 | 0.6 | 0.6 | 0.0 | 152.0 | 12.4 | 6.2 |
| 9/17/2018 | 1.7 | | 0.5 | | 0.1 | 100.8 | 16.3 | 6.3 |
| 9/24/2018 | 2.6 | 2.5 | 0.6 | 0.6 | 0.1 | 146.1 | 17.4 | 6.4 |
| 10/1/2018 | 3.2 | 2.8 | 0.6 | 0.6 | 0.1 | 118.1 | 17.3 | 6.3 |
| 10/8/2018 | 4.7 | 4.3 | 0.7 | 0.7 | 0.1 | 93.8 | 17.0 | 6.4 |
| 10/15/2018 | 1.9 | 1.0 | 0.3 | 0.2 | 1.0 | 128.2 | 16.3 | 6.4 |
| 10/22/2018 | 1.7 | 0.9 | 0.1 | 0.1 | 3.2 | 136.1 | 14.2 | 6.5 |
| 10/29/2018 | 0.9 | 0.6 | 0.1 | 0.1 | 4.3 | 166.1 | 12.0 | 6.7 |

**Table S3.** Regression models for $O_2$ consumption vs metal flux in descending order of best fit, as determined by the lowest AIC.

| | Model Type | Equation | Parameter Values | $R^2$ | AICc |
|---|---|---|---|---|---|
| **Total Fe** | Exponential 2P | $a * e^{b*O_2}$ | a= 297.97±83.63±<br>b=-0.000632±0.0003468 | 0.45 | 93.1 |
| | Mechanistic Growth | $a * (1 - b * e^{-c*O_2})$ | a= 586.17±167.1<br>b = 0.78±0.25<br>c=-0.00303±0.00307 | 0.66 | 120.4 |
| | Logistic 3P | $\frac{c}{1 + e^{-a*(O_2-b)}}$ | a = -0.005588±0.0053015±<br>b = -152.04±161.2<br>c= 563.6±134.4 | 0.62 | 121 |
| **Soluble Fe** | Exponential 2P | $a * e^{b*O_2}$ | a= 285.0±95.8<br>b=-0.000763±0.000395 | 0.49 | 95.3 |
| | Mechanistic Growth | $a * (1 - b * e^{-c*O_2})$ | a= 619.7±160.8<br>b =0.94±0.27<br>c=-0.00362±0.0031 | 0.72 | 121.6 |
| | Quadratic | $a + b * O_2 + C * O_2^2$ | a=11.38±161.6<br>b=-1.04±0.65<br>c=-0.00049±0.00049 | 0.67 | 122.64 |
| **Total Mn** | Mechanistic Growth | $a * (1 - b * e^{-c*O_2})$ | a= 44.9±15.6<br>b = 1.13±34.2<br>c=-0.027±2.7 | 0.33 | 101 |
| | Quadratic | $a + b * O_2 + C * O_2^2$ | a = 18.52±29.2<br>b = -0.097±0.117<br>c=-7.13*10$^{-5}$±8.87*10$^{-5}$ | 0.31 | 102 |
| **Soluble Mn** | Mechanistic Growth | $a * (1 - b * e^{-c*O_2})$ | a= 44.9±15.6<br>b = 1.13±50.1<br>c=-0.027±3.9 | 0.32 | 101 |
| | Quadratic | $a + b * O_2 + C * O_2^2$ | a = 19.1±29.3<br>b = -0.097±0.1177<br>c=-0.000072±8.9*10$^{-5}$ | 0.19 | 102 |

**B. Historical Volume Weighted Hypolimnetic Metal Conditions**

2016 and 2017 VWH total and soluble Fe and Mn concentrations (Figure S5) were calculated using the same method as described in the methods for 2018 data. For both 2016 and 2017 the HOx system was run continuously for the stratification periods. In 2016, VWH Fe concentrations are higher than in 2017 with maximum total Fe concentrations of 158 kg and 42 kg in 2016 and 2017 respectively. However, VWH Mn concentrations are similar between 2016 and 2017 with maximum total Mn concentrations of 25 kg and 27 kg between 2016 and 2017 respectively. Both Fe and Mn concentrations follow a similar pattern in both years with a buildup of Fe and Mn concentrations in the late stratification period.

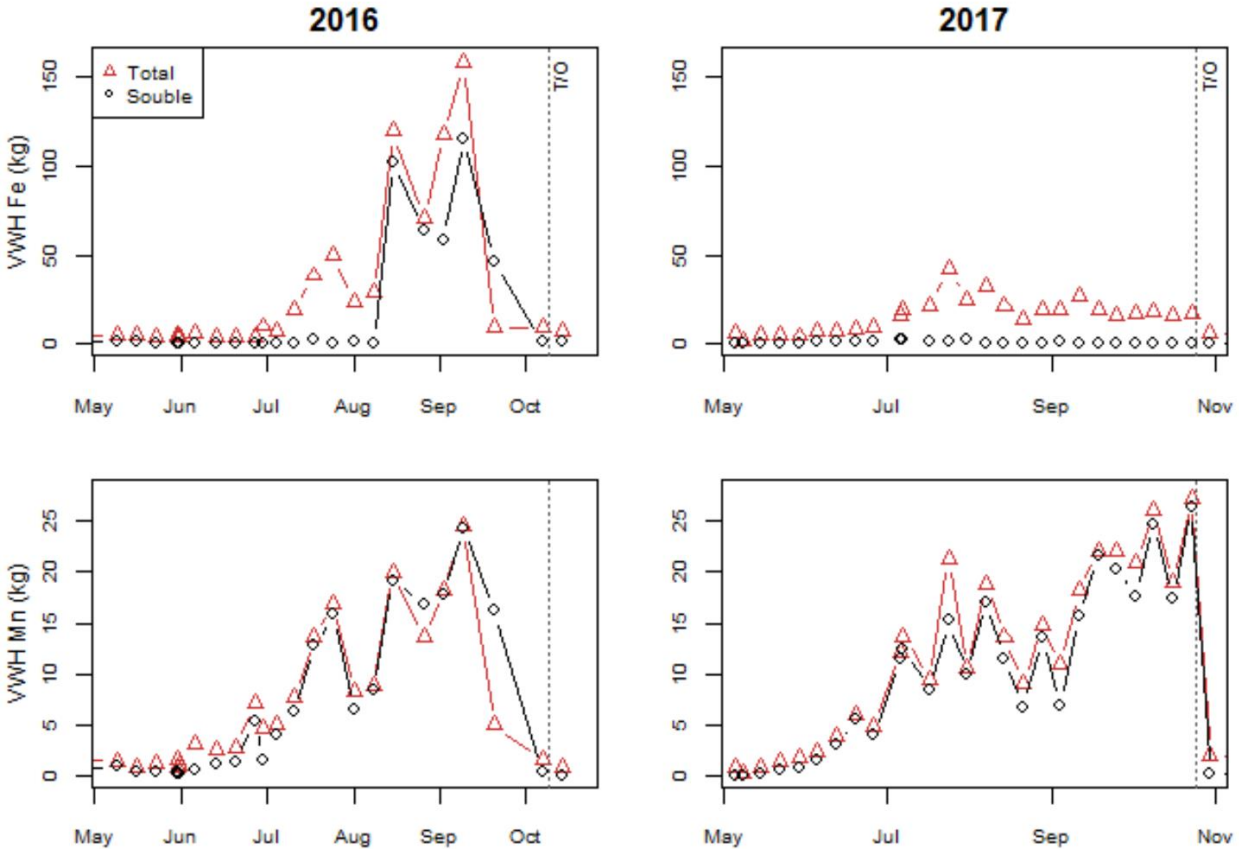


**Figure S5.** Volume weighted hypolimnetic concentrations of total (red triangle) and soluble (black circle) for FCR in 2016 and 2017. Average thermocline depth was 5.0 m for both years